Polarizable Force Field Development and Molecular Dynamics Simulations of Ionic Liquids

ARTICLE *in* THE JOURNAL OF PHYSICAL CHEMISTRY B · AUGUST 2009

Impact Factor: 3.3 · DOI: 10.1021/jp905220k · Source: PubMed

1 AUTHOR:

Oleg Borodin
Army Research Laboratory
182 PUBLICATIONS **4,136** CITATIONS

Polarizable Force Field Development and Molecular Dynamics Simulations of Ionic Liquids

Oleg Borodin*

Wasatch Molecular Inc., 2141 St. Marys Drive, Ste 102, Salt Lake City, Utah 84108, and Department of Materials Science & Engineering, 122 South Central Campus Drive, Room 304, University of Utah, Salt Lake City, Utah 84112-0560

Received: June 3, 2009; Revised Manuscript Received: July 10, 2009

A many-body polarizable force field has been developed and validated for ionic liquids (ILs) containing 1-methyl-3-alkylimidazolium, 1-alkyl-2-methyl-3-alkylimidazolium, *N*-methyl-*N*-alkylpyrrolidinium, *N*-alkylpyridinium, *N*-alkyl-*N*-alkylpiperidinium, *N*-alkyl-*N*-alkylmorpholinium, tetraalkylammonium, tetraalkylphosphonium, *N*-methyl-*N*-oligoetherpyrrolidinium cations and BF_4^-, $CF_3BF_3^-$, $CH_3BF_3^-$, $CF_3SO_3^-$, PF_6^-, dicyanamide, tricyanomethanide, tetracyanoborate, bis(trifluoromethane sulfonyl)imide (Ntf_2^- or $TFSI^-$), bis(fluorosulfonyl)imide (FSI^-) and nitrate anions. Classical molecular dynamics (MD) simulations have been performed on 30 ionic liquids at 298, 333, and 393 K. The IL density, heat of vaporization, ion self-diffusion coefficient, conductivity, and viscosity were found in a good agreement with available experimental data. Ability of the developed force field to predict ionic crystal cell parameters has been tested on four ionic crystals containing Ntf_2^- anions. The influence of polarization on the structure and ion transport has been investigated for [emim][BF_4] IL. A connection between the structural changes in IL resulting from turning off polarization and slowing down of ion dynamics has been found. Developed force field has also provided accurate description/prediction of thermodynamic and transport properties of alkanes, fluoroalkanes, oligoethers (1,2-dimethoxyethane), ethylene carbonate, propylene carbonate, dimethyl carbonate, hydrazine, methyhydrazine, dimethylhydrazine, acetonitrile, dimethyl amine, and dimethyl ketone.

1. Introduction

Room temperature ionic liquids (ILs) have attracted significant attention from the scientific community over the past decade.[1] ILs have been widely investigated for a variety of applications including solvents for synthetic and catalytic applications,[2] lubricants,[3,4] lithium batteries,[5−8] actuators,[9,10] sensors,[11] reaction media,[12] replacement of conventional solvents,[13] active pharmaceutical ingredients,[12] and hypergolic propellants.[14] The negligible vapor pressure, good thermal and electrochemical stability, good dissolution with many organic and inorganic compounds, low flammability,[15] and a wide variety of possible anions and cations are a few examples of the properties that make ILs exciting alternative materials for many applications. Importantly, IL properties can be tailored for specific chemical (separation, catalysis, reactions, propellants, explosives) or electrochemical (battery, actuators, supercapacitors) applications by tuning the combination of cations and anions to achieve the desired thermodynamic, solvating, and transport properties. For example, higher charge delocalization improves ion transport,[16,17] and the length and nature of substituted groups affect melting (T_m) and glass transition (T_g) temperatures as well as thermal stability.[18,19]

The availability of a large number of cations and anions for ILs presents tremendous opportunities for finding optimal cation/anion pairs and IL mixtures for the design of ILs targeted toward specific applications. However, screening a large number of possible cation/anion combinations also presents an enormous challenge for product design as synthesis, purification, and characterization of a large number of ILs are expensive. Efficient and reliable predictive tools can speed up the development cycle not only by providing expedient predictions of properties for specific ILs and IL mixtures, but also by providing an improved fundamental understanding of ILs and data needed for the development of empirical structure−property relationship models. A number of empirical correlations for IL properties have been recently suggested such as the dependence of the degree of dynamic ion correlation on anionic donor ability (Lewis basicity), hydrogen bond donor acidity,[20] and relationship between solvent polarity and molar volumes.[21] Other studies[22,23] suggested that various molecular orbital, thermodynamic, and electrostatic descriptors also influence IL melting temperature (T_m), density, and dielectric properties.[23] The speed of sound has been correlated with the surface tension and density.[24] Similarly, a correlation between the heat of vaporization and surface tension has been proposed.[25] Group contribution methods[26,27] have also shown some success in describing density and viscosity[28] (with errors often less than 28%) for a number of ILs. However, hydrogen-bonded ILs have been shown to require special modification of the group contribution method.[29] So far, it has proved challenging to develop generic correlations between chemical structure and thermodynamic and particularly transport properties of ILs especially when novel groups are introduced in the IL structure indicating a need for new methods that can take into account all details of the chemical structure.

Molecular dynamics (MD) simulations are emerging as a good complementary (to empirical correlations) option for reliable prediction of IL properties. Indeed, most structural, thermodynamic, and transport properties of ILs are readily accessible from simulations. Realization of the potential power of MD simulations in predicting properties and assisting in obtaining fundamental understanding of ILs has

* To whom correspondence should be addressed. E-mail: Oleg.Borodin@utah.edu.

10.1021/jp905220k CCC: $40.75
Published on Web 07/28/2009

sparked tremendous interest in this field leading to numerous MD simulation studies reported on ILs with imidazolium,[30−59] pyridinium,[60] pyrrolidinium,[61−63] triazolium,[64,65] tetraalkylphosphonium,[66] and tetraalkylammonium,[67−69] cations, and an variety of anions have provided valuable insights that have led to improved understanding of IL structure, transport, and interactions of IL with lithium salts[48,49] and fluids such as CO_2,[70,71] water,[32] and methane.[32] Central to accurate prediction of IL properties from MD simulations is the quality of the force field used. Unfortunately, many researchers[37,44,47,72−74] have provided little or no validation of the force field used in their simulations of ILs leaving open the question of how well the underlying structure, thermodynamics, and transport properties are predicted by simulations. Other groups[40,41,46,61,75−78] have developed force field specifically for a very narrow set of ILs of their interest and have validated it against available experimental data. The latter studies are often limited to one or perhaps a few ILs. While they can provide valuable understanding of the properties of the specific ILs, it is not clear whether the same force field can be utilized for simulations of other ILs that are composed from similar functional groups or have a different anion/cation combination. Effective utilization of MD simulations in the design of new materials heavily relies on accuracy, reliability, and particularly transferability of the force field, properties that are largely untested and unproven for existing IL force fields.

Only a few groups led by Padua, Canongia Lopes, and Maginn, Acevedo have made consistent efforts in constructing IL force fields that would be applicable beyond a few compounds of interest, while tens of other groups reported MD simulations for a few ILs only. Canongia Lopes and Padua developed a force field for ILs covering the broadest set of cations[40,41,45,48,50,52,61,75,77,79−83] such as imidazolium$^+$ including trialkylimidazolium$^+$ and alkoxycarbonyl-imidazolium$^+$, pyridinium$^+$, phosphonium$^+$ and anions such as alkylsulfonate$^-$, alkylsulfate$^-$, bis(trifluoromethane sulfone imide) (TFSI or Ntf_2), bis(fluorosulfonyl)amide (FSI^-), chloride, bromide, and dicyanamide$^-$ ($N(CN)_2^-$ or dca^-) anions. While the number of ILs included in the force field reported by this group is impressive and IL density and crystal phase cell parameters are well reproduced, the ability of this force field to predict heat of vaporization and transport properties is much less so. For example, the enthalpy of vaporization for [emim][Ntf_2] was found approximately 20 kJ/mol higher[84] than values obtained from three independent experimental measurements.[57] The self-diffusion coefficients obtained from simulations using the force field of Padua et al. were a factor of 5 smaller than experimental values for [emim][Ntf_2].[57] Balasubramanian's group has utilized Padua's force field in their simulations and concluded[56] that for [mmim][Cl] and [bmim][PF_6], simulations were not able to accurately reproduce details of the cation and anion coordination. Moreover, the ion transport in ILs was found to be quite sluggish compared to experiments. Similarly sluggish transport has been found in simulations by Picálek et al.[59] of [emim][PF_6], [bmim][PF_6], and [bmim][BF_4] utilizing five different force fields. Sambasivarao and Acevedo[85] have recently published an OPLS-AA type force field for 1-alkyl-3-methylimidazolium, *N*-alkylpyridinium, and choline cations, along with Cl^-, PF_6^-, BF_4^-, NO_3^-, $AlCl_4^-$, $Al_2Cl_7^-$, Ntf_2^-, saccharinate, and acesulfamate anions reporting good agreement for density, but no transport properties were given.

Maginn's group has also constructed a force field for a number of ILs.[32,42,43,60,64,86−90] A force field developed by Maginn's group has been validated against experimental data on self-diffusion coefficients, heat capacity, melting points, and viscosity. While for some ILs such as [emim][Ntf_2] and [bmim][PF_6] simulations using Maginn's force field have yielded good agreement with experimental data, unlike results for Padua's force field, there is a number of alkylpyridinium-based ionic liquids for which predicted apparent self-diffusivities are roughly 10 times lower than experimental values.[60] Interestingly, in some simulations[56,91] of [alkylimidazolium][PF_6], reduced ion charges of $0.9e$ and $0.8e$ (e = electron charge) were used. We speculate that the reduction of ion charges and Coulomb interactions has helped to achieve an improved description of IL transport properties. However, it is not necessary to reduce ion charges to achieve good description of IL transport. For example, Micaelo et al.[51] have taken a different route by setting the cation and anion charges to $1e$ and $-1e$ and optimizing F−F and O−O Lennard-Jones parameters for PF_6^- and NO_3^- to match experimental density, self-diffusion coefficient, and viscosity data for [bmim][PF_6] and [bmim][NO_3] ILs. They assumed a very low 0.001−0.01 kJ/mol values for the well depth for P−P and N−N (of NO_3^-) Lennard-Jones interaction. While highly successful in describing density and transport properties of [bmim][PF_6] and [bmim][NO_3] Micaelo's force field predicted heat of vaporization (H^{vap}) of 123.3 and 130.2 kJ/mol for these ILs, respectively, at 298 K. These predicted simulation H^{vap} values seem to be lower than the experimental estimates[25] of ∼168 kJ/mol for these ILs indicating a possible pitfall in the otherwise excellent force field. One should keep in mind that the experimental H^{vap} data were extrapolated from ∼500 to 298 K.

There are only a few instances when a developed IL force field has been shown to accurately describe IL density, heat of vaporization, ion transport, and viscosity. Loddermann, Paschek, and Ludwig's[57] force field for [alkylimidazolium]-[Ntf_2] ILs is a clear example of such a success. In summary, we note that the development of the IL force field that is capable of predicting thermodynamics, structural, and transport properties for a wide range of ILs is a difficult task that is far from being complete despite an exponentially increasing number of IL simulation papers.

An objective of this work is to develop a force field that would be applicable to a wide class of ILs and validate the ability of MD simulations using this force field to reproduce/predict density, heat of vaporization, ion self-diffusion coefficient, ionic conductivity, and viscosity of ILs in a liquid state. A limited investigation of the ability of the developed force field to predict IL crystal structures will also be reported but will be extended in the future work. This force field is envisioned as an integral part of the Atomistic Polarizable Potential for Liquids, Electrolytes, & Polymers (APPLE&P) force-field database that is currently under development in our group. Figure 1 shows types of anions and cations chosen for this endeavor. This particular set of ions covers a range of popular ILs, for which experimental data necessary for the force field validation are available in the literature. Quite importantly, ions shown in Figure 1 also allow us to thoroughly investigate the force-field transferability by combining various groups in a number of ways without changing the repulsion−dispersion nonbonded parameters. As the repulsion−dispersion are the only parameters that are fit to experimental data we consider transferability of these parameters between various compounds and chemical environments to be of critical importance for the predictive capabilities of the developed force field and APPLE&P database. The repulsion−dispersion parameter transferability is tested by modifying BF_4^-

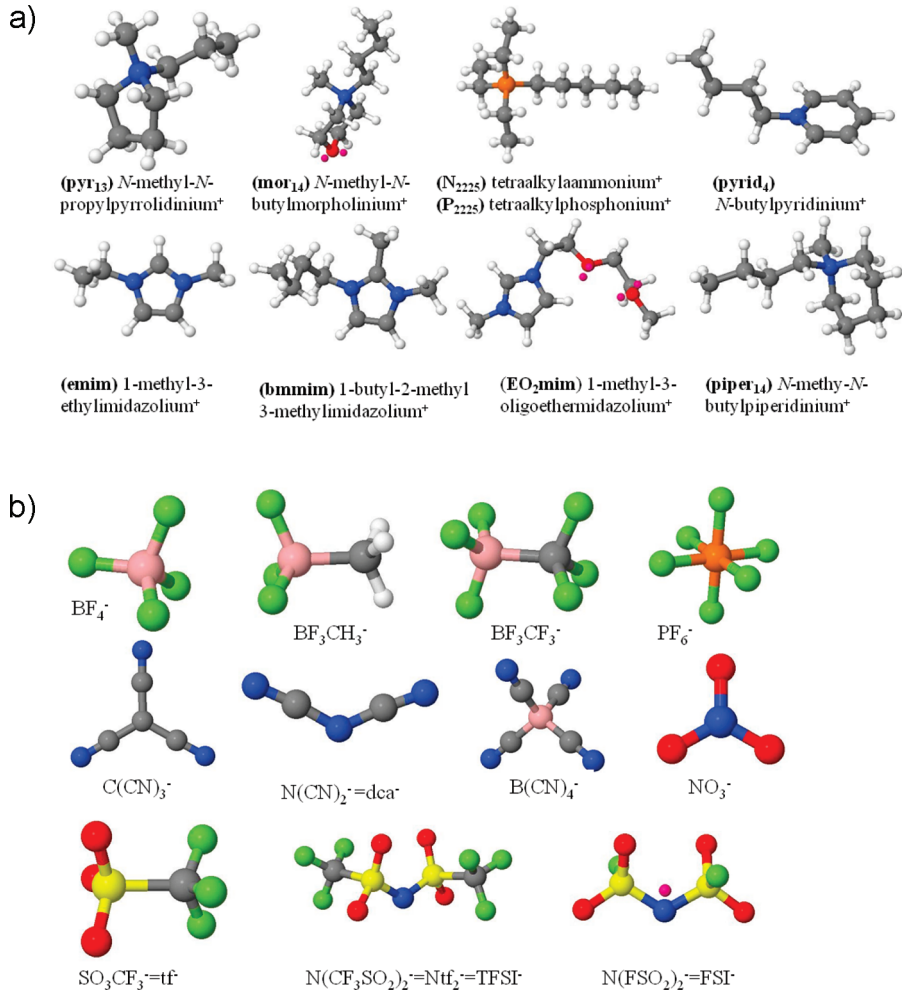

Figure 1. A representative set of anions and cations for which the many-body polarizable force field has been developed.

anion with $-CF_3^-$ or $-CH_3^-$ groups resulting in $CH_3BF_3^-$ or $CF_3BF_3^-$ anions or by changing anion from $TFSI^-$ or Ntf_2 or $(CF_3SO_2)_2N^-$ to FSI^-═$(FSO_2)_2N^-$ and to $CF_3SO_3^-$ while keeping the repulsion−dispersion parameters for oxygen, fluorine, and sulfur the same, or by increasing the size of the alkyl tail, or by changing alkyl tails to oligoethers, therefore introducing hydrogen bonding and strong dipolar interactions in ILs. Considering $N(CN)_2^-$, $C(CN)_3^-$, $B(CN)_4^-$ anions allowed us to test transferability of the cyano group repulsion−dispersion parameters. Many of the chosen anions such as $TFSI^-$, FSI^-, $N(CN)_2^-$, $C(CN)_3^-$, $BF_3CF_3^-$ with broad charge delocalization have been chosen because they yield ILs with low melting and glass transition temperatures, relatively low viscosity, and fast ion transport, which are desired for numerous applications.

2. Force-Field Development Methodology

The following form of the force field relating the potential energy $U^{tot}(\mathbf{r})$ to atomic coordinates $\mathbf{r}$ for the ensemble of atoms has been chosen. It is split into nonbonded $U^{NB}(\mathbf{r})$ and bonded contributions as given by

$$U^{tot}(\mathbf{r}) = U^{NB}(\mathbf{r}) + \sum_{bends} U^{BEND}(\theta_{ijk}) + \sum_{dihedrals} U^{DIHEDRAL}(\phi_{ijkl}) + \sum_{\substack{improper \\ dihedrals}} U^{IMP}(\phi_{ijkl}^{imp}) \quad (1)$$

where the sums are over all bonds, bends, dihedrals, and improper dihedrals in the system. The contributions to the potential energy due to bonds, bends, dihedrals, and out-of-plane bending (improper dihedrals) are

$$U^{BEND}(\theta_{ijk}) = \frac{1}{2}k_{\alpha\beta\gamma}^{BEND}(\theta_{ijk} - \theta_{ijk}^0)^2 \quad (2)$$

$$U^{DIHEDRAL}(\phi_{ijkl}) = \sum_n \frac{1}{2}k_{\alpha\beta\gamma\delta,n}^{DIHEDRAL}[1 - \cos(n\phi_{ijkl})] \quad (3)$$

$$U^{IMP}(\phi_{ijkl}^{imp}) = \frac{1}{2}k_{\alpha\beta\gamma\delta}^{IMP}(\phi_{ijkl}^{imp})^2 \quad (4)$$

where θ_{ijk} and θ_{ijk}^0 are the instantaneous and natural bending angles for atoms i, j and k; ϕ_{ijkl} is the dihedral angle for atoms i, j, k, and l; and ϕ_{ijkl}^{imp} is the out-of-plane bending angle for an sp^2 center at atom j. The strength of these interactions is characterized by the corresponding force constants $k_{\alpha\beta\gamma}^{BEND}$, $k_{\alpha\beta\gamma\delta,n}^{DIHEDRAL}$, and $k_{\alpha\beta\gamma\delta}^{IMP}$, respectively. The subscripts α, β, γ, and δ denote atom type for atoms i, j, k, and l, respectively.

The nonbonded energy $U^{NB}(\mathbf{r})$ consists of the sum of two-body repulsion and dispersion energy terms $U^{RD}(\mathbf{r})$, the energy due to interactions of fixed charges $U^{coul}(\mathbf{r})$, and the polarization

energy $U^{pol}(\mathbf{r})$ arising from the interaction between induced dipoles with fixed charges and other induced dipoles,

$$U^{NB}(\mathbf{r}) = U^{RD}(\mathbf{r}) + U^{coul}(\mathbf{r}) + U^{pol}(\mathbf{r}) = \sum_{i>j}\left(A_{\alpha\beta}\exp(-B_{\alpha\beta}r_{ij}) - C_{\alpha\beta}r_{ij}^{-6} + D\left(\frac{12}{B_{\alpha\beta}r_{ij}}\right)^{12}\right) + \sum_{i>j}\left(\frac{q_iq_j}{4\pi\varepsilon_0 r_{ij}}\right) - \frac{1}{2}\sum_i \vec{\mu}_i\cdot\vec{E}_i^0 \quad (5)$$

where $\vec{\mu}_i = \alpha_i\vec{E}_i^{tot}$ is an induced dipole at force center i, α_i is the isotropic atomic polarizability, $\vec{E}_i^{tot}$ is the total electrostatic field at the atomic site i due to permanent charges q_j and induced dipoles $\vec{\mu}_j$, ε_0 is the dielectric permittivity of vacuum, $\vec{E}_i^0$ is the electric field due to fixed charges only, $A_{\alpha\beta}$ and $B_{\alpha\beta}$ are the repulsion parameters and $C_{\alpha\beta}$ is the dispersion parameter for interaction between atoms i and j with atom types α and β. The term $D(12/B_{\alpha\beta}r_{ij})^{12}$, with $D = 5 \times 10^{-5}$ kcal/mol for all pair interactions, is essentially zero at typical nonbonded atomic separations, but becomes the dominant term at $r_{ij} < 1$ Å, ensuring that $U^{RD}(\mathbf{r})$ is repulsive at distances much smaller than the size of an atom. Intramolecular nonbonded interactions are included for atoms separated by three or more covalent bonds. We used Thole screening[92] ($a_T = 0.2$) that smears induced dipoles in order to prevent the so-called "polarization catastrophe" from occurring. The intramolecular interaction between an induced dipole and a partial charge separated by three bonds was scaled by 0.8. Finally, for heteroatom interactions, the modified Waldman−Hagler combining rules[92] were used

$$A_{ij} = \sqrt{A_{ii}A_{jj}}\frac{B_{ij}^{\,6}}{B_{ii}^{\,3}B_{jj}^{\,3}}; \quad B_{ij} = \left(\frac{2}{B_{ii}^{-6} + B_{jj}^{-6}}\right)^{1/6}; \quad C_{ij} = \sqrt{C_{ii}C_{jj}} \quad (6)$$

These combining rules have been successfully used by us for simulations of liquids,[92,93] polymers, electrolytes,[92,94] and ionic liquids.[62,63,95,96]

A, B, and C parameters can be expressed in terms of potential well depth ε, the interatomic separation at the minimum R*, and the steepness parameter λ as given by eq 7−9

$$A = 6\varepsilon(\exp\lambda)/(\lambda - 6) \quad (7)$$

$$B = \lambda/\mathrm{R}^* \quad (8)$$

$$C = \varepsilon\lambda(R^*)^6/(\lambda - 6) \quad (9)$$

We followed the previously described force-field development methodology[62,92] that is briefly summarized here. First, atomic polarizabilities are determined by fitting to the molecular polarizability of in the gas phase determined from quantum chemistry (QC) calculations and by fitting the polarization contribution to the binding energy for the interaction of anions with a 1e charge and cations with the −1e charge. Second, partial charges are fit to describe the electrostatic potential on a grid of points around a molecule, as well as molecular gas phase dipole moment, all obtained from QC calculations. Third, bond lengths and natural bending angles are fit to reproduce the gas-phase geometries obtained from quantum chemistry, while bending force constants are either taken from previously developed force fields or fit to the energy for the bending angle distortions obtained from quantum chemistry. Finally, dihedral angle parameters are determined by fitting the gas phase conformational-energy surface of model molecules as determined from quantum chemistry.

Partial Atomic Charges. To establish partial atomic charges, the electrostatic potentials on grids of evenly spaced points (~10^5 points) around the low-energy gas-phase conformers as well as the dipole moments $\vec{\mu}_i$ of these molecules were calculated at the MP2/aug-cc-pvDz level, except for anions for force field version greater than f1e12. The MP2/cc-pvTz level was used for the later. Charge-bond increments were used to calculate partial atomic charges. The value q_i of the partial charge positioned on atom i is calculated as a sum of all charge-bond increments that involve atom i, as shown in eq 10.

$$q_i = \sum_j^{n\mathrm{Bonds}} \delta_{ij} \quad (10)$$

A set of charge-bond increments ($\vec{\delta}$) was determined by minimizing the objective function

$$\chi^2(\vec{\delta}) = \sum_{i=1}^{M}\left[\sum_{j=1}^{N_{GRID}}\frac{\omega^{\phi}}{N_{GRID}}(\phi_{ij}^{QC} - \phi_{ij}^{FF}(\vec{\delta}))^2 + \omega^{\vec{\mu}}(\vec{\mu}_i^{QC} - \vec{\mu}_i^{FF}(\vec{\delta})^2)^2\right] \quad (11)$$

where ϕ_{ij}^{QC} and ϕ_{ij}^{FF} are the electrostatic potential for the ith molecule (or complex) at the jth grid point from QC and the developed force field (FF), respectively, $\vec{\mu}_i^{QC}$ and $\vec{\mu}_i^{FF}$ are dipole moments for molecule i. The relative weights for fitting electrostatic potential and the dipole moments were set to 1.0 and 0.1, respectively. The electrostatic potential for points closer than 1.8 Å to oxygen and fluorine, 1.5 Å to hydrogen, 2.5 Å to carbon atoms, and 2 Å for all other atoms were excluded from the fitting, as were points further than 4 Å away from any atom.

A lone pair (Lp, type 2) has been added to oxygen atoms in C−O−C bends in oligoethers and carbonates as previously discussed.[97] The length of the Lp−O bond (0.65 Å) and Lp−O−Lp angle (102°) were fit in order to obtain the best description of the electrostatic potential around 1,2-dimethoxyethane (DME). It also has been found that the description of electrostatic potential around a FSI^- anion could improved by a almost a factor of 2 by placing an additional force center with a partial charge (denoted Lp, type 1) in the plane of S−N−S bend as shown in Figure 1. Placing a set to two additional force centers at the positions, where lone pairs are expected on the nitrogen atom, yielded a less significant improvement in the description of the electrostatic potential around FSI^- compared to adding one extended partial charge as shown in Figure 1. Two set of force fields have been derived for the FSI^- anion, one with an extended charge (Lp) and the other one without it. In the case of the Ntf_2^- anion, an addition of an extended charge resulted in a less significant improvement of the electrostatic potential grid description, therefore, an extended charge center has not been included in the Ntf_2^- force field.

Valence Parameters. Bond lengths were set to the average of the values for the corresponding bond type obtained from QC calculations at the B3LYP/aug-cc-pvDz or M05−2X/aug-cc-pvDz level for cations and neutral molecules, and M05−2X/cc-pvTz or M06/cc-pvTz level for anions. Bond lengths were

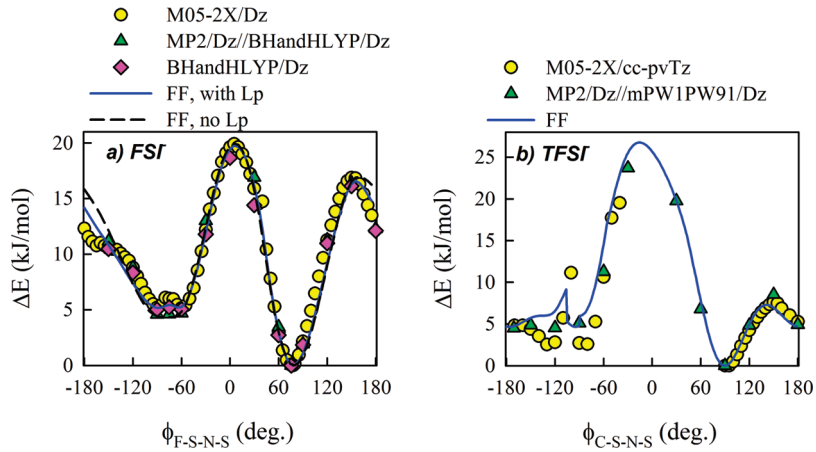

Figure 2. Dihedral drives for FSI^- (a) and Ntf_2^- (or $TFSI^-$) (b) anions from quantum chemistry and molecular mechanics using developed force field (FF). Dz denotes aug-cc-pvDz basis set.

constrained in MD simulations except for BF_4^- and PF_6^- anions, for which harmonic springs were used. The QC calculations using triple-ζ basis sets for anions were chosen over aug-cc-pvDz basis set as triple-ζ basis sets yielded a consistently better agreement with the bond lengths extracted from X-ray measurements of ionic crystals. The natural bending angles (θ^0_{ijk}) were fit to the bending angles of the optimized QC geometries. The torsional (dihedral) parameters were fit to energetics from MP2/aug-cc-pvDz//B3LYP/aug-cc-pvDz or MP2/aug-cc-pvDz//M05-2X/aug-cc-pvDz levels except for FSI^- and Ntf_2^- (or $TFSI^-$) anions as discussed below. During the initial part of the project improved M05-2X and M06 density functionals were not available, and the B3LYP density functional was used for geometry optimization.

The scans of FSI^- and NTf_2^- ($TFSI^-$) dihedral angles were performed at a number of levels of theory in QC calculations as shown in Figure 2 with all degrees of freedom relaxed except for those shown in Figure 2. The aug-cc-pvDz (Dz) and cc-pvTz basis sets were utilized for geometry optimization unlike the previous work where HF/6-31G* level was used for geometry optimization.[61] Figure 2 indicates that M05-2X/Dz density functional yields similar results to MP2/Dz calculations. Both $TFSI^-$ (Ntf_2^-) and FSI^- show two minima with the least stable minima being split. During scans of C−S−N−S dihedral of $TFSI^-$ a discontinuity was observed at −90° in M05-2X/cc-pvTz calculations and at −105° at molecular mechanics calculations. At the discontinuity point the second C−S−N−S angle jumps from 74° to 129° in M05-2X/cc-pvTz calculations and from 87° to 177° in the molecular mechanics drive using developed force field. We consider force field fits to QC dihedral angle scans to be excellent for FSI^- anion and good for $TFSI^-$ anion.

Repulsion−Dispersion Parameters. Fitting repulsion−dispersion (R/D) interactions parameters (A, B, C in eq 5 or ε, λ, R^* in eqs 7−9) is the most challenging and controversial part of force field development because they can be obtained by fitting to a number of different data sets yielding somewhat different potentials. The most often used data for fitting the repulsion−dispersion parameters are crystal structures together with sublimation energies, liquid densities, and heats of vaporization (H^{vap}), vapor−liquid equilibrium data, and gas-phase dimer binding energies obtained from QC calculations or from the symmetry-adapted perturbation theory quantum chemistry calculations. In this work we fit the R/D parameters to the density and H^{vap} of nonionic liquids, while the density and dynamic properties instead of heat of vaporization were utilized for fitting IL-specific R/D parameters. We opted to utilize transport properties of ILs for fitting R/D parameters instead of H^{vap} as transport properties are more readily available and reliable for a variety of ILs, while H^{vap} data are scarce for ILs and are often obtained at high temperature (500 K) followed by an extrapolation to room temperature. Moreover, a noticeable difference was reported between H^{vap} for ILs obtained using different techniques.[57] In the case of determining the C···C and H···H R/D parameters for *n*-alkanes we also utilized the self-diffusion coefficients from pfg-NMR experiments in addition to the density and H^{vap} to ensure that an accurate description of dynamic properties is also achieved. To achieve a good description of the thermodynamic and transport properties for *n*-alkanes the R/D parameters for carbon atoms at chain ends ($-CH_3$ groups) were allowed to be slightly different from those for the interior carbons. Specifically, the van-der-Waals well depth ε (see eqs 7−9) for the C_m type (in CH_3- groups) was 11% deeper than that for interior carbon atoms, while R^* and λ were the same. Table 1 lists the R/D types used in simulations of nonionic and ionic liquids together with the properties and compounds used for their fitting. Tables 2 and 3 give a list of simulated nonionic and ionic liquids, respectively. The R/D parameters were fit to liquids in the following order: *n*-alkanes (yielding parameters for carbon and hydrogen atoms), fluoroalkanes (yielding parameters for fluorine atoms while using C and C_m from *n*-alkanes), 1,2-dimethoxyethane (DME) (yielding oxygen parameters), dimethyl amine, hydrazine, and methyl hydrazine (yielding nitrogen and hydrogen connected to a nitrogen parameters). The sp^3 (hybridized) carbon R/D parameters were applied to the sp^2 carbon atoms because the predicted density and H^{vap} of benzene using these parameters were found to be acceptable as shown in Table 2. The sp hybridized carbon parameters were required for simulations of ILs containing cyano groups. We fit the *sp* carbon R/D parameters to acetonitrile (ACN). Transferability of the sp carbon R/D parameters from ACN to alkynes such as 2-butyne was tested and found to be marginal as density of 2-butyne from MD simulations deviated by 3% from experimental data, while a good prediction of the 2-butyne heat of vaporization has been observed as seen from Table 2. Thus, the sp carbon parameters will need to be further refined for the force fields targeting alkyne liquids, while these R/D parameters are expected to perform satisfactory for ILs containing cyano groups.

Fitting the R/D parameters for the nitrogen bearing a formal positive charge in IL cations is complicated because the IL density and transport properties are relatively insensitive to these

TABLE 1: The Repulsion−Dispersion (R/D) Types and a List of Compounds and Properties[a] Used for Their Fitting

label	atom R/D types	compounds used for fitting	properties used for fitting
C, C_c	sp^3 and sp^2 carbon, C^- in $C(CN)_3^-$	$C_{10}H_{22}$	ρ, ΔH^{vap}, D
C_m	sp^3 carbon at chain ends (CH_3-, CF_3- groups)	C_3H_8, C_5H_{12}	ρ, ΔH^{vap}, D
C_t	sp carbon	acetonitrile	ρ, ΔH^{vap}
H	H connected to C	$C_{10}H_{22}$, C_5H_{12}	ρ, ΔH^{vap}, D
H_n	H connected to N	hydrazine, methyl hydrazine	ρ, ΔH^{vap}
N	neutral nitrogen, nitrogen with the formal charge −1e	hydrazine, methyl hydrazine	ρ, ΔH^{vap}
n^+,N^+	nitrogen with the formal charge +0.5e and +1e	relation $R^* \approx (\text{polarizability})^{0.25}$ was used yielding $R^*_{N+} = 0.726\ R^*_N$ for pyrrolidinium	
O, O=	all oxygen atoms (−O−, O=C, O=S)	1,2-dimethoxyethane, propylene carbonate	ρ, ΔH^{vap}
F	all fluorine atoms	C_4F_{10}, C_6F_{14}	ρ, ΔH^{vap}
B^-	B in BF_4^-	[emim][BF_4]	ρ, D
S, S^-	sulfur in CF_3SO_3, Ntf_2^- and FSI^-	[emim][CF_3SO_3]	ρ, D
P^-	in PF_6^-	[emim][PF_6]	ρ, D
P^+	in tetraalkylphosphonium cations	[$P_{2,2,2,5}$][Ntf_2]	ρ, λ

[a] ρ (density), ΔH^{vap} (heat of vaporization), D (self-diffusion coefficient), λ (ionic conductivity).

TABLE 2: Liquid Density (ρ), Heat of Vaporization (H^{vap}) and Self-Diffusion Coefficient (D) from MD Simulations and Experiments (in Parentheses) at 1 atm. The Deviations of MD Data from Experimental Data Are Given as $\Delta\rho$, ΔH^{vap}, ΔD

liquid	T (K)	ρ^{MD} (ρ^{exp}) (kg/m^3)	$\Delta\rho$ (%)	H^{vap}_{MD}(H^{vap}_{exp}) (kcal/mol)	ΔH^{vap} (%)	D^{MD} (D^{exp}) (10^{-10} m/s^2)	ΔD (%)	ref to exp. data
C_3H_8	321	575 (581)	−1.0	4.29 (4.55)	−6	57.3 (54.7)	−5	116, 116, 117
C_5H_{12}	298	617 (621)	−0.6	6.09 (6.39)	−5	59 (56.2)	−5	116, 116, 118
C_6H_{14}	298	651 (655)	−0.6	7.33 (7.58)	−3			116, 116
$C_{10}H_{22}$	298	729 (727)	0.3	12.25 (12.28)	0	13.1 (14)	−6	116, 116, 119
2-butyne	293	715 (691)	3.0	6.53 (6.41)	2			120, 121
C_6H_6	298	861 (874)	−1.5	7.82 (8.)	−2.3	22.9		122
C_4F_{10}	273	1557 (1585)	−1.7	5.35 (5.46)	−2			6,123
C_6F_{14}	298	1663 (1675)	−0.7	7.31 (7.51)	−3			123
C_9F_{20}	295	1785 (1769)	0.9					123
1,2-dimethoxyethane (DME)	298	851.2 (861)	−1.1	8.63 (8.70)	−1	32.9 (31.5)	4	116, 122, 124
Diglyme	298	928 (934)	−0.6			13.7 (13)	5	122, 124
dimethylamine (DMA)	273	686 (680)	0.8	6.36 (6.37)	0	42.5 + 8.8		122
dimethylnitramine (DMNA)	345	1116 (1109)	0.6	11.65		15.6		122
hydrazine	298	1009 (1004)	0.5	10.68 (10.68)	0			122
methylhydrazine	298	871 (870)	0.1	9.77 (9.65)	1			116, 122
dimethylhydrazine	298	800 (791[a])	1.1	8.09 (8.42)	−4			116, 122
propylene carbonate (PC)	303	1209 (1194)	1.3	13.5 (14.4[b])		5.4 + 0.9 (5.8)	8	124−126
ethylene carbonate (EC)	313	1302 (1321)	−1.5	13.8		7.8 + 1.2 (8.0)	13	122, 124
dimethyl carbonate (DMC)	298	1040 (1057)	−1.4	8.88 (9.01)	−1	22 + 3.4 (26)	−2	122, 124, 127
dimethyl ketone	298	778 (785)	−0.8	6.85 (7.47)	−8	39.9 + 6.8 (37.5−40.9)		122, 122
acetonitrile (ACN)	298	769 (777)	−1.0	7.8 (7.98)	−2	38.5 + 6.4		116, 128

[a] At 22 °C. [b] At 25 °C.

$N^+\cdots N$ R/D parameters. Indeed, the N^+ atoms are largely shielded from the direct repulsive interactions with the anions. For example, the closest anion atom approaching N^+ of *N*-propyl-*N*-methyl pyrrolidinium$^+$ cation in [pyr_{13}][Ntf_2] IL is around 4 Å,[62] which is larger than the R^* in eq 7−9, thus, explaining the weak sensitivity of IL properties to the repulsive parameters of $N^+\cdots N^+$ interactions. Because of the low sensitivity of IL properties to the $N^+\cdots N^+$ R/D parameters we opted for using an empirical correlation between the atom size and its polarization given by eq 12.[98]

$$R^*(N^+)/R^*(N) \approx (\alpha(N^+)/\alpha(N))^{0.25} \qquad (12)$$

where R^* is the position of the minimum of van-der-Waals interactions (see eq 7−9) and α is the atomic polarizability. Specifically, we reduced the size of N^+ by 27% compared to R^*(N) using the polarization of N in a neutral molecule and N^+ in the alkylpyrrolidinium cation. We did not use eq 12 to obtain the R/D parameters for $P^+\cdots P^+$ interactions because the IL transport properties and density of [P_{2225}][Ntf_2] were sensitive enough to the R/D parameters that the later could be fit. It would seem logical to apply the same relation between R^* and α (eq 12) for the atoms in anions. However, we have not done so in this version of the force field for two reasons: (1) polarization of an anion in a condensed phase has been shown[99] to be significantly (up to 37% for Cl^- in water) reduced from the gas-phase value, (2) large basis sets with multiple augmentations (diffuse functions) are needed to accurately calculate polarization from QC calculations. In this work we used the $N\cdots N$ R/D parameters for $N^-\cdots N^-$ in anions, except for the revised (f1e14) version of nitrate anion. In the f1e14 version, the $N^-\cdots N^-$ parameters for nitrate anion were fit to density and transport properties of [bmim][NO_3]. The $S^-\cdots S^-$ parameters were fit to [emim][CF_3SO_3] density and self-diffusion coefficients. Atom type definitions and atomic polarizabilities are summarized in Supporting Information. Force field parameters are available to academic groups for noncommercial research at no cost upon signing a license agreement from Wasatch Molecular Inc.

3. Molecular Dynamics Simulations

A version of the MD simulation package *Lucretius* that includes many-body polarization was used for all MD simula-

TABLE 3: Density (in kg m^{-3}) of 30 ILs Predicted from MD Simulations Performed, Experimental Values[a] (in Parentheses) Followed by the Deviation $\Delta\rho$% of MD Simulation Predictions from Experiments (in bold) ($\Delta\rho$)

Ionic Liquid	393 K ρ^{MD} (ρ^{exp}) $\Delta\rho$%	333 K ρ^{MD} (ρ^{exp}) $\Delta\rho$%	298 K ρ^{MD} (ρ^{exp}) $\Delta\rho$%	exp. ref
[emim][BF_4]	1198 (1206) **−0.6**	1243 (1253) **−0.8**	1262 (1280) **−1.4**	129
[bmim][BF_4]	1128 (1135) **−0.6**	1169 (1178) **−0.8**	1193 (1201.6−1204)	17, 130
[bmim][PF_6]	1286 (1288) **−0.2**	1336 (1341) **−0.3**	1365 (1371) **−0.4**	17
[emim][Ntf_2]	1425 (1427) **−0.1**	1479 (1487) **−0.6**	1511 (1522) **−0.7**	19
[bmim][Ntf_2]	1349 (1348) **0.1**	1401 (1404) **−0.2**	1433 (1437) **−0.2**	131
[C_6mim][Ntf_2]	1290	1342 (1330) **0.9**	1373 (1366) **0.5**	19
[C_7mim][Ntf_2]	1266 (1262) **0.3**	1317 (1314) **0.2**	1346 (1348) **0.1**	132
[bmmim][Ntf_2]	1331	1383 (1386) **−0.2**	1413 (1420) **−0.5**	109
[bmim][CF_3SO_3]	1217 (1226) **−0.7**	1262 (1274) **−0.9**	1287 (1302) **−1.1**	17
[bmim][NO_3] (f1c)	1106 (1092) **1.3**	1141 (1131,1136)	1166 (1154) **1.1**	133, 134
[bmim][NO_3] (f1e14)	1092 (1092) **0.2**	1132 (1131,1136)	1155 (1154) 0.1	133, 134
[emim][CF_3BF_3]	1246	1291	1321	
[emim][CH_3BF_3]	1093 (1091) **0.2**	1130 (1130) **0.0**	1155 (1153) **0.2**	135
[emim][$N(CN)_2$]	1018	1055	1077 (1080) **−0.2**	136
[bmim][$N(CN)_2$]	986	1021	1042 (1058) **−1.5**	137
[emim][$C(CN)_3$]	1007	1046	1069, (1060 ± 5%), (1110 at 293K)	138, 139
[EO_2mim][BF_4]	1186	1232	1259 (1260) **0.1**	101
[EO_2mim][Ntf_2]	1368	1423	1455 (1450) **0.4**	101
[emim][FSI(noLp)]	1312	1359	1389	
[emim][FSI (Lp)]	1312	1359	1389	
[pyr_{13}][Ntf_2]	1347 (1343) **0.3**	1391 (1384) **0.7**	1424 (1408−1447)	110, 140
[pyr_{14}][Ntf_2]	1314 (1313) **0.1**	1364 (1367) **−0.2**	1394 (1399) **−0.4**	108
[$pyr_{1,1O2}$][Ntf_2][b]	1374	1422	1455 (1454) **0.1**	141
[pyr_{13}][FSI(noLp)] (small)	1233	1276	1302	
[pyr_{13}][FSI(noLp)] (big)	1233	1275		
[pyr_{13}][FSI (Lp)] (big)	1234	1276	1305	
[pyr_{12}][$N(CN)_2$]	977	1011	1032 (1060) **−2.7**	136
[P_{2225}][Ntf_2]			1300 (1320) **−1.5**	142
[N_{1114}][Ntf_2]	1325	1377 (1357) **1.4**	1408 (1393) **1.1**	108
[$piper_{14}$][Ntf_2]	1302	1351	1378 (1378.6−1380)	109, 143
[$pyrid_4$][Ntf_2]	1370 (1366) **0.3**	1420 (1422) **−0.1**	1454 (1454) **0.0**	108
[$pyrid_4$][BF_4]	1148	1189 (1192) **−0.3**	1213 (1214) **−0.1**	144
[$mor_{1,2}$][Ntf_2]	1356	1405	1434 (1440.5) **−0.4**	141
[emim][$B(CN)_4$]	990	1034	1059	

[a] Some of the data have been extrapolated to higher temperatures using published fits to experimental data. [b] 1O2 denotes a $CH_3OCH_2CH_2-(N^+)$ tail.

tions.[100] A three-dimensional, periodic cubic simulation cell consisting of 125−180 ion pairs was simulated for all ILs with the exception of [pyr_{13}][Ntf_2], [P_{2225}][Ntf_2], and [pyr_{13}][FSI]. Two simulation cells were set up for [pyr_{13}][FSI] comprising 100 and 216 ion pairs in order to investigate the influence of the simulation cell size on the IL thermodynamic and transport properties. The exact number of IL ion pairs used in simulation is given in Supporting Information for all ILs. The IL initial configurations were created in the gas phase corresponding to a cell (linear) dimension of approximately 75−90 Å. The dimensions of the simulation cells were reduced to yield estimated densities at 393 K followed by 0.8−2 ns NPT run. The average box sizes from the NPT runs were utilized in the subsequent NVT production runs for all ILs except for [emim][CF_3BF_3] and [emim][CH_3BH_3] for which the results from NPT simulations are reported. The length of production runs was always long enough to achieve the diffusive regime in ILs and ranged from 4 to 64 ns except for the most recent simulations of [bmim][NO_3] using revised force field f1e14. The Supporting Information section provides the simulation lengths for all simulated temperatures. Previously reported[101] density and self-diffusion coefficients from MD simulations for [EO_2mim][Ntf_2], [EO_2mim][BF_4], and [C_7mim][Ntf_2] ILs are also reported here for completeness.

The Ewald summation method was used for electrostatic interactions between partial charges with partial charges and partial charges with induced dipole moments using k^3 from 6^3 to 8^3 k-vectors, and α from 8.5−9.5 Å. The interaction between an induced dipole and a partial charge separated by three bonds was scaled by 0.8, providing an improved description of the electrostatic potential around the molecules. Multiple time step integration with an inner time step of 0.5 fs (bonded interactions), a central time step of 1.5 fs for all nonbonded interactions within a truncation of 7.0 Å, and an outer time step of 3.0 fs for all nonbonded between 7.0 Å and the nonbonded truncation distance of 10.5 or 11 Å as well as for the reciprocal part of Ewald was employed. A Nose−Hoover thermostat (NPT and NVT simulations) and a barostat (NPT simulations) were used to control the temperature and pressure with the associated frequencies of 10^{-2} and 0.5×10^{-3} fs. Induced dipoles were calculated via a direct iteration with a predictor method. Pressure tensor and virial were calculated using atom-based with bond (constrained) forces.

Brownian dynamics simulations of ion pairs were performed at 298 K for 1−4 ns to yield gas phase ion pair energies. The number of simulated ion pairs was the same as in the simulation box used for simulating the liquid phase.

Crystal simulations were performed on [emim][Ntf_2], [emim][CF_3SO_3], [pyr_{13}][Ntf_2] and [pyr_{14}][Ntf_2] ionic crystals using an orthorhombic version of the simulation code at N**P**T ensemble, where diagonal components of the **P** stress tensor were set to 1 atm. The experimental coordinates were used as an initial configuration. Simulation cell consisted of 128, 256, 216, and 144 ion pairs for [emim][Ntf_2], [emim][CF_3SO_3], [pyr_{13}][Ntf_2], and [pyr_{14}][Ntf_2] ionic crystals, respectively. Ionic crystals were equilibrated for 0.2 ns followed by production

TABLE 4: Crystal Lattice Parameters for Selected Ionic Crystals from MD Simulations and X-ray Experiments.[145−147]

	lattice parameters and cell volume			
	a (Å)	*b* (Å)	*c* (Å)	cell vol (Å^3)
	[emim][Ntf_2] at 230 K			
MD	18.78	8.62	19.19	3107
X-ray[145]	18.50	8.63	19.26	3073
deviation (%)	1.5	0.0	−0.3	1.1
	[pyr_{13}][Ntf_2] at 200 K			
MD	12.98	15.45	17.39	3487
X-ray[146]	12.82	15.51	17.32	3444
deviation (%)	1.2	−0.4	0.4	1.3
	[pyr_{14}][Ntf_2] at 125.1 K			
MD	8.48	12.88	16.79	1834
X-ray[147]	8.39	13.01	16.58	1811
deviation (%)	1.0	−1.0	1.2	1.3
	[emim][CF_3SO_3] at 150 K			
MD	10.26	12.35	18.68	2366
X-ray[145]	10.18	12.38	18.29	2307
deviation (%)	0.7	−0.3	2.1	2.5

runs of 0.5 ns. The same Ewald parameters and integrators as in the liquid phase simulations have been utilized.

4. Thermodynamic and Structural Parameters

Density. Table 3 summarizes the density of ILs predicted from MD simulations and its deviation from experiments. In most cases we observed excellent predictive capabilities of the developed force field with the difference between predicted and measured values of less than 1%. For a few ILs density from MD simulations deviated up to 2%; however, for those, ILs experimental data contained only three digits such as 1.06 g/cm^3 for [pyr_{12}][$N(CN)_2$] indicating at least 1% error bar. Thus, we suspect that the larger deviation between experimental densities and those from simulations could be due, in part, to low accuracy of experimental values for [pyr_{12}][$N(CN)_2$].

Crystal Structure. We have performed a limited investigation of the ability of MD simulations using a developed force field to predict ionic crystal cell parameters and volume for four ionic crystals: [emim][Ntf_2], [emim][CF_3SO_3], [pyr_{13}][Ntf_2], and [pyr_{14}][Ntf_2]. Ionic crystals with the orthorhombic cells have been chosen because of the limitations of our polarizable code, which could not handle arbitrary flexible cells at the time of when simulations were performed. Ionic crystal cell parameters and volume from MD simulations are reported in Table 4. Good agreement is observed for cell parameters for all simulated ionic crystals. Note, that while the orthorhombic symmetry was constrained during simulations the off-diagonal pressure tensor components were less than a few atm indicating that no shear stresses developed during simulations. To ensure that not only cell parameters are well predicted in MD simulations but the atomic packing is well reproduced, we calculated positions of Ntf_2^- anion oxygen atoms from MD simulations around cations and compared it with that from X-ray measurements. Figure 3 shows that the packing of Ntf_2^- anion oxygen atoms around cations from MD simulations is in good agreement with the positions extracted from X-ray experiments.

Heat of Vaporization. A negligible vapor pressure makes ILs especially attractive for numerous applications. On the other hand, a high heat of vaporization (H^{vap}) creates additional challenges associated with an accurate measurement of H^{vap} for ILs, and, therefore, validation of H^{vap} predicted from MD simulations. Heat of vaporization values of [$C_n$mim][Ntf_2] ILs have been reported from numerous experiments and simulations.

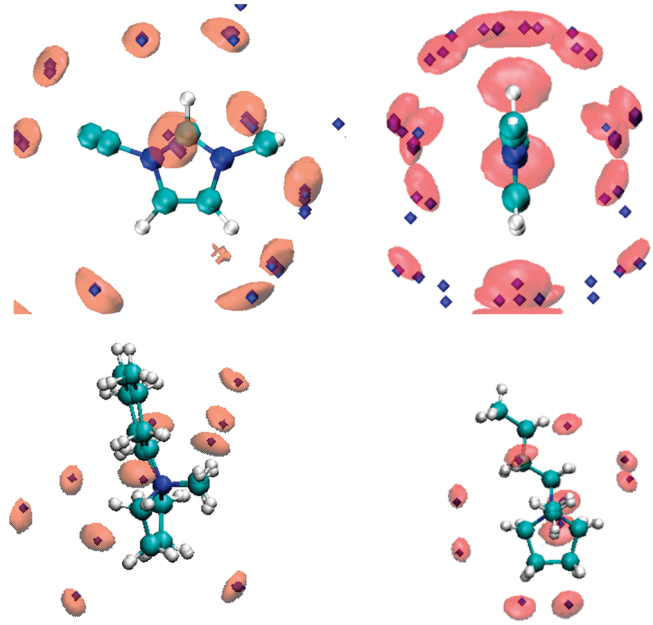

Figure 3. Isosurface of O atom of Ntf_2^- anion for $\rho/\rho^{random} = 50$ (volume distribution function) for [emim][Ntf_2] and [pyr_{14}][Ntf_2] from MD simulations (red isosurface) and experiments[147] (blue isosurface). The average structure of pyr_{14}^+ cation from both MD simulations and experiments is shown.

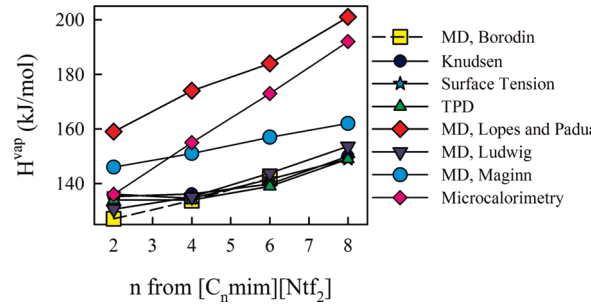

Figure 4. Heat of vaporization for ILs from experiments (microcalorimetry,[84] Knudsen, surface tension, TPD[102]) taken from ref 57 compared to MD simulation predictions by Ludwig group,[57] Lopes and Padua,[84] Maginn group,[88] and from current work (Borodin).

The MD simulation predictions and data from the vacuum−vaporization drop microcalorimetric experiments were reported in Santos et al.[84] and are shown in Figure 4. These MD simulations utilized the force field developed by Padua and Canongia Lopes.[81] The H^{vap} from microcalorimetric experiments predicted a strong (8.9 kJ/mol for −CH2− group from experiments) increase of H^{vap} with the increasing alkyl tail. MD simulations by Padua predicted a slightly smaller increase of H^{vap} with an increase of alkyl tail length but reported higher absolute values for H^{vap}. Maginn's group[87] have reported much smaller H^{vap} values and a smaller increase of H^{vap} per $-CH_2-$ group compared to Canongia Lopes and Padua simulations. At the same time, Ludwig's group reported H^{vap} from MD simulations and compared them to the most recent experiments as shown in Figure 4. Ludwig simulations results agreed well with the majority of experiments except for the microcalorimetric data. Our MD simulations predictions are also shown in Figure 4. An excellent agreement between our predictions and results of TPD,[102] Knudsen,[103] and surface tension experiments is observed. Note, that $H^{vap} = 127.1$ kJ/mol predicted from our MD simulations is slightly lower than experimental values of 134−136 kJ/mol but is similar to the value of 130.6 kJ/mol reported by Ludwig's group.[57] Canongia Lopes and Padua group

TABLE 5: Heat of Vaporization (in kJ mol^{-1}) Predicted from MD Simulations ILs at 298 K

ionic liquid	H^{vap}	ionic liquid	H^{vap}
[emim][BF_4]	135.3	[emim][FSI]	132.9
[bmim][BF_4]	140.8	[emim][FSI (noLp)]	132.1
[bmim][PF_6]	150.6	[pyr_{13}][Ntf_2]	143.6
[emim][Ntf_2]	127.7	[pyr_{14}][Ntf_2]	147.6
[bmim][Ntf_2]	133.7	[$pyr_{1,1O2}$][Ntf_2]	138.5
[C_6mim][Ntf_2]	141.9	[pyr_{13}][FSI]	147.0
[bmmim][Ntf_2]	133.0	[pyr_{13}][FSI (noLp)] (small)	144.3
[bmim][CF_3SO_3]	142.7	[pyr_{12}][$N(CN)_2$]	133.2
[bmim][NO_3] (f1c)	151.7	[P_{2225}][Ntf_2]	151.3
[emim][CF_3BF_3]	130.2	[N_{1114}][Ntf_2]	157.1
[emim][CH_3BF_3]	123.3	[$piper_{14}$][Ntf_2]	156.2
[emim][$N(CN)_2$]	125.9	[$pyrid_4$][Ntf_2]	137.3
[bmim][$N(CN)_2$]	132.0	[$pyrid_4$][BF_4]	145.6
[emim][$C(CN)_3$]	135.1	[mor_{12}][Ntf_2]	158.9
[EO_2mim][Ntf_2]	132.3	[emim][$B(CN)_4$]	137.7

has reported a much higher value of $H^{vap} = 159$ kJ/mol, while Maginn group has reported only a slightly higher value of 143 kJ/mol compared to our simulations. We predict an increase of H^{vap} of 3.3−4.1 kJ/mol per $-CH_2-$ tail group in good agreement with Maginn and Ludwig simulations but in a sharp contrast to results reported by Canongia Lopes and Padua.

Table 5 summarizes MD simulations predictions of H^{vap} for the other ILs. Experimental data exist only for a few of ILs, thus allowing only a limited validation of simulations results. Our MD simulation prediction of H^{vap} for [emim][BF_4] and [bmim][BF_4] of 135.3 and 140.8 kJ/mol are in line with the value of 128.2 kJ/mol for [bmim][BF_4] obtained from the most recently reported empirical correlation with the surface tension.[25] To compare our data to the experimental H^{vap} 162 ± 3 kJ/mol for [C_8mim][BF_4] obtained from TPD experiments[102] we take the difference of H^{vap} for [emim][BF_4] and [bmim][BF_4] of 5.5 kJ/mol and extrapolate H^{vap} to [C_8mim][BF_4]. The extrapolated MD simulation value of 151.8 kJ/mol is slightly lower than the TPD[102] experimental value of 162 ± 3 kJ/mol for [C_8mim][BF_4]. Most of the reported simulation studies yielded much higher H^{vap} values, Wu et al.[46] reported H^{vap} of 175.4 kJ/mol for [bmim][BF_4], while Liu et al.[76] have reported 179.2 kJ/mol. Raabe et al.[104] reported H^{vap} of 182.2 and 188.2 kJ/mol for [emim][BF_4] and [bmim][BF_4], respectively. Sambasivarao and Acevedo[85] have recently extended the OPLS−AA force field for ILs and reported H^{vap} of 75.3 kJ/mol for [emim][BF_4] and 116.3 kJ/mol for [bmim][BF_4]. Sambasivarao and Acevedo[85] considered these predictions to be in good agreement with experiments; we think that their simulation predictions not only predict suspiciously large contribution of 20 kJ/mol per $-CH_2-$ tail group but also underestimate the absolute value of H^{vap}.

Our simulation prediction of H^{vap} of 150.6 kJ/mol for [bmim][PF_6] is lower than the TPD experimental[102] value of 169 kJ/mol for [C_8mim][PF_6] owing to shorter alky−alkyl in the simulated IL compared to the experimental one. The most recent empirical correlation[25] of H^{vap} with surface tension yielded H^{vap} of 154.8 kJ/mol for [bmim][PF_6], which is in good agreement with our MD simulation predictions of 150.6 kJ/mol. Numerous simulations of [bmim][PF_6] have been reported. Two MD simulations yielded lower H^{vap} using a value of 123.3 kJ/mol reported for GROMOS FF.[51] Sambasivarao et al.[85] reported a value of 133.5 kJ/mol, while Liu et al.[76] reported much higher H^{vap} values of 190.4 kJ/mol (united atom FF) and 186.7 kJ/mol (all atom FF). H^{vap} prediction from this work for [bmim][CF_3SO_3] of 142.7 kJ/mol is consistent with H^{vap} from TPD experiment[102] of 151 ± 3 kJ/mol for [C_8mim][CF_3SO_3] after the correction for a longer alkyl tail length used in experiments is made. H^{vap} from this work is higher than H^{vap} =

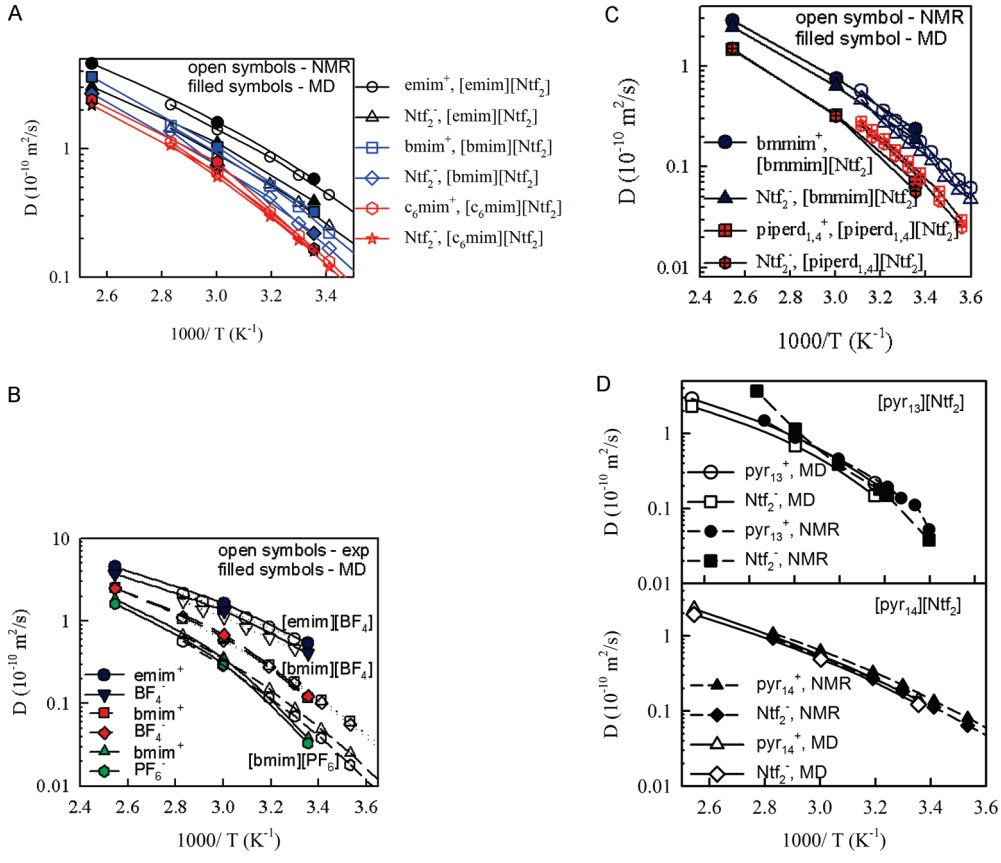

Figure 5. Ion self-diffusion coefficients of ILs obtained from MD simulations and NMR experiments.[17,108,110,156]

TABLE 6: The Ion Self-Diffusion Coefficients (in 10^{-10} m^2/s) from MD Simulations, Experimental Values[a] (In Parentheses) Followed by the Deviation in % of MD Simulation Predictions from Experiments (in Bold) (ΔD)

ionic liquid		393 K D^{MD}	333 K D^{MD} (D^{exp}) ΔD	298 K D^{MD} (D^{exp}) ΔD	ΔD^{FSC} (%)	exp. ref
[emim][BF_4]	D_+	3.89	1.39 (1.35) **3**	0.480 (0.497) **−3**	16	129
	D_-	3.21	1.14 (1.16) **−2**	0.362 (0.416) **−13**		
[bmim][BF_4]	D_+	2.15	0.55 (0.59) **−7**	0.101 (0.145) **−30**	14−17	17
	D_-	2.13	0.59 (0.59) **−7**	0.105 (0.134) **−22**		
[bmim][PF_6]	D_+	1.61	0.30 (0.365) **−17**	0.032 (0.069) **−56**	10−21	17, 148
	D_-	1.43	0.26 (0.284) **−9**	0.028 (0.0515) **−45**		
[emim][Ntf_2]	D_+	4.13	1.42 (1.37) **4**	0.516 (0.495) **4**	10−13	19
	D_-	2.74	1.00 (0.90) **10**	0.347 (0.309) **13**		
[bmim][Ntf_2]	D_+	3.17	0.907 (0.904) **0**	0.289 (0.275) **5**	12−14	17
	D_-	2.35	0.654 (0.750) **−13**	0.196 (0.218) **−10**		
[C_6mim][Ntf_2]	D_+	2.15	0.706 (0.643) **10**	0.149 (0.168) **−11**	13	19
	D_-	1.96	0.595 (0.603) **−1**	0.144 (0.153) **−6**		
[bmmim][Ntf_2]	D_+	2.68	0.71 (0.93) **−24**	0.18 (0.198) **−9**	8−11	109
	D_-	2.33	0.59 (0.72) **−18**	0.14 (0.152) **−5**		
[bmim][CF_3SO_3]	D_+	2.06	0.42 (0.690) **−39**	0.112 (0.179) **−38**	16−20	17
	D_-	1.68	0.36 (0.590) **−39**	0.093 (0.143) **−35**		
[bmim][NO_3] (f1c)	D_+	1.27	0.16	0.020	14−30	
	D_-	1.53	0.17	0.020		
[bmim][NO_3] (f1e12)	D_+	1.59	0.34			
	D_-	1.96	0.39			
[emim][CF_3BF_3]	D_+	4.69	1.41	0.449	12	
	D_-	3.17	1.00	0.321		
[emim][CH_3BF_3]	D_+	3.96	1.41	0.449	16	
	D_-	3.43	1.00	0.321		
[emim][$N(CN)_2$]	D_+	4.57	2.31	0.898	12−21	
	D_-	4.90	2.82	1.41		
[bmim][$N(CN)_2$]	D_+	4.08	1.08	0.37	13	
	D_-	4.60	1.43	0.45		
[emim][$C(CN)_3$]	D_+	5.48	1.74	0.649	14−17	
	D_-	6.08	2.04	0.702		
[EO_2mim][BF_4]	D_+	1.78	0.37	0.080		
	D_-	2.45	0.47	0.094		
[EO_2mim][Ntf_2]	D_+	2.77	0.71	0.0169		
	D_-	2.60	0.63	0.0173		
[emim][FSI(noLp)]	D_+	3.83	1.74	0.752	12−18	
	D_-	3.45	1.58	0.673		
[emim][FSI]	D_+	4.52	1.68	0.82		
	D_-	3.90	1.43	0.64		
[pyr_{13}][Ntf_2]	D_+	2.49	0.764	0.183 (0.26) **−30**	16−18	110
	D_-	1.79	0.587	0.125 (0.17) **−27**		
[pyr_{14}][Ntf_2]	D_+	1.97	0.46 (0.64) **−27**	0.119 (0.177) **−33**	17	108
	D_-	1.65	0.42 (0.53) **−21**	0.104 (0.142) **−27**		
[$pyr_{1,1O2}$][Ntf_2]	D_+	2.30	0.69	0.173	11−19	
	D_-	2.02	0.54	0.126		
[pyr_{13}][FSI(noLp)] (small)	D_+	1.85	0.50	0.181	16−24	
	D_-	2.20	0.64	0.201		
[pyr_{13}][FSI(noLp)] (big)	D_+	1.75	0.50		14	
	D_-	2.08	0.61			
[pyr_{13}][FSI] (big)	D_+	1.85	0.54	0.14		
	D_-	2.29	0.63	0.20		
[pyr_{12}][$N(CN)_2$]	D_+	2.45	0.75		14−20	136
	D_-	4.09	1.39			
[P_{2225}][Ntf_2]	D_+			0.085	19	142
	D_-			0.101		
[N_{1114}][Ntf_2]	D_+	1.96	0.450 (0.538) **−16**	0.103 (0.131) **−21**	13−18	108
	D_-	1.61	0.453 (0.487) −7	0.093 (0.117) **−21**		
[$piper_{14}$][Ntf_2]	D_+	1.30	0.267 (0.438) **−39**	0.055 (0.106) **−48**	16−18	109
	D_-	1.47	0.287 (0.397) **−28**	0.062 (0.087) **−29**		
[$pyrid_4$][Ntf_2]	D_+	2.48	0.797 (0.795) **0**	0.234 (0.217) **8**		108
	D_-	2.32	0.608 (0.654) **−7**	0.181 (0.177) **2**		
[$pyrid_4$][BF_4]	D_+	1.80	0.286 (0.426) **−33**	0.046 (0.091) **−50**	10−34	149
	D_-	2.00	0.288 (0482) **−40**	0.052 (0.103) **−49**		
[mor_{12}][Ntf_2]	D_+	1.21	0.203	0.038	15−22	
	D_-	1.31	0.199	0.043		
[emim][$B(CN)_4$]	D_+	4.24	1.13	0.32		
	D_-	3.62	1.01	0.29		

[a] Some of the data have been extrapolated to higher temperatures using published fits to experimental data.

130 kJ/mol for [bmim][CF_3SO_3] from MD simulations by Sambasivarao et al.[85]

Heats of vaporization were also experimentally measured for ILs containing $N(CN)_2^-$ and NO_3^- anions. Emel'yanenko et al.[105] has reported heats of vaporization of 163.7 ± 5.3 and 162.4 ± 5.7 kJ/mol for [emim][NO_3] and [bmim][NO_3], respectively. The MD simulation prediction of H^{vap} for [bmim][NO_3] from this work is 151.7 kJ/mol, which is slightly lower than

TABLE 7: Conductivity (λ in mS/cm) of ILs Predicted from MD Simulations Performed, Experimental Values[a] (in Parentheses) Followed by the Deviation $\Delta\lambda$% of MD Simulation Predictions from Experiments (in Bold)

ionic liquid	393 K λ^{MD}	333 K λ^{MD} (λ^{exp}) $\Delta\lambda$%	298 K λ^{MD} (λ^{exp}) $\Delta\lambda$%	exp. ref
[emim][BF_4]	109	38.5 (35.6) **8**	16.2 (13.6−15.7)	129
[bmim][BF_4]	38.5	12.5 (14.1) **−11**	2.77 (3.53,4.38)**−22,−37**	17, 130
[bmim][PF_6]	32.2	6.11 (6.79) **−10**	0.76 (1.49) **−49**	17
[emim][Ntf_2]	56.4	22.4 (21.4) **4**	9.05 (9.0) **10**	19
[bmim][Ntf_2]	33.6	11.9 (11.2) **6**	4.17 (3.88) **7**	131
[C_6mim][Ntf_2]	20.2	9.6 (7.27) **33**	2.5 (2.2) **13**	19
[EO_2mim][Ntf_2]			2.75	
[bmmim][Ntf_2]	26.8	8.40 (4.90) **71**	2.60 (1.60) **63**	109
[bmim][CF_3SO_3]	32.3	8.81 (9.49) **−7**	2.04 (2.88) **−29**	17
[bmim][NO_3]	29.0	4.34	0.70	
[emim][CF_3BF_3]	95.9	39.5	18.8 (14.6) **29**	150
[emim][CH_3BF_3]	97.1	33.8	12.1 (9.0) **35**	135
[emim][$N(CN)_2$]	105	59.5 (55.7) **25**	33.6 (28.4) **18**	136
[bmim][$N(CN)_2$]	87.2	30 (24.1) **24**	10.7 (11) **−3**	136
[emim][$C(CN)_3$]	135	50.3 (44.3) **14**	19.9 (21.7) **−8**	138, 139
[emim][FSI(noLp)]	73.0	38.5	20.5 (15.4, 17.74@293K)	151, 152
[emim][FSI]	91.4	36.9	18.2 (15.4, 17.74@293K)	151, 152
[pyr_{13}][Ntf_2]	35.1	13.5 (6.42) **110**	3.9 (3.9)**0**	110
[pyr_{14}][Ntf_2]	25.5	7.0 (8.7) **−20**	2.2 (2.75) **−20**	108
[$pyr_{1,1O2}$][Ntf_2]	33.1	10.5	3.2 (3.7) **−14**	141
[pyr_{13}][FSI(noLp)] (small)	34.6	12.8 (13.4) **−4**	5.5 (6.4,8.2, 9.14@293K)	151−153
[pyr_{13}][FSI(noLp)] (big)	35.6	12.3 (13.4) **−8**		
[pyr_{13}][FSI] (big)	43.2	14.4 (13.4) **8**	4.6 (6.4,8.2, 9.14@293K)	151−153
[pyr_{12}][$N(CN)_2$]	90.1	24.5 (39) **−37**	11.2 (20.1) **−45**	136
[P_{2225}][Ntf_2]			1.34 (1.73) **−23**	142
[N_{1114}][Ntf_2]	26.8	7.76 (7.37) **5**	1.82 (2.05) **−11**	108
[$piper_{14}$][Ntf_2]	18.1	4.4 (4.2) **3**	1.0 (1.1, 1.2)	109, 141
[$pyrid_4$][Ntf_2]	33.3	10.1 (8.7) **17**	3.7 (2.75) **33**	108
[$pyrid_4$][BF_4]	41.8	7.8 (8.5) **−8**	1.5 (1.9) **−22**	149
[mor_{12}][Ntf_2]	19.3	3.2	0.60 (0.40) **49**	141
[emim][$B(CN)_4$]	76.4	27.1 (35.8) **−24**	10.5 (15.7) **−33**	154

[a] Some of the data have been extrapolated to higher temperatures using published fits to experimental data.

TABLE 8: Viscosity (in mPa s) of ILs Predicted from MD Simulations Performed, Experimental Values[a] (in Parentheses) Followed by the Deviation $\Delta\eta$% of MD Simulation Predictions from Experimental Values (in Bold)

ionic liquid	393 K η^{MD}	333 K η^{MD} (η^{exp}) $\Delta\eta$%	298 K η^{MD} (η^{exp}) $\Delta\eta$%	exp. ref
[emim][Ntf_2]	4.2	9.1 (11.6)	31.2 (32.2) **−3**	19
[bmim][CF_3SO_3]	7.8	25 (21.7) **15**	90 (84.2) **7**	17
[bmim][NO_3] (f1c)	12.3	73 (37) **98**	250 (194) **22**	133
[emim][$N(CN)_2$]	2.2	5.0 (6.5) **−23**	13.3 (16.1) **−17**	136
[emim][$C(CN)_3$]	2.4	6.1	19.8 (18 @293 K)	139
[emim][FSI(noLp)]	3.5	9.4	13.5 (15.5) **−13**	151
[pyr_{13}][Ntf_2]	6.1	13.2	76 (61) **25**	151
[pyr_{14}][Ntf_2]	6.5	16.6 (21.0) **−21**	78 (75.7) **3**	108
[$pyr_{1,1O2}$][Ntf_2]	4.7	23.5	56 (53) **6**	141
[pyr_{13}][FSI(noLp)]	7.3	20.7 (16.7) **24**	80 (39−40)	151, 153
[pyr_{12}][$N(CN)_2$]	4.85	13.4 (9.8) **37**	45 (25.8) **74**	136
[P_{2225}][Ntf_2]			80 (88) **−9**	142
[N_{1114}][Ntf_2]	6.1	29.3 (24.2) **21**	93 (99) **−6**	108
[$piper_{14}$][Ntf_2]	7.4	37 (39) **−7**		109, 143
[$pyrid_4$][Ntf_2]	4.5	11.2 (16.3) **−32**	38 (56.7) **−33**	149
[mor_{12}][Ntf_2]	9.5	36		141
[emim][$B(CN)_4$]	3.3	9.6 (6.8) **41**	37 (20) **85**	155

[a] Some of the experimental densities have been extrapolated to higher temperatures using relations provided by authors.

Emel'yanenko et al.[105] results. Emel'yanenko et al.[105] also reported that MD simulations of Kelkar and Maginn predicted H^{vap} of 159 kJ/mol for [bmim][NO_3] in agreement with the experimental data. A much lower value of 130.2 kJ/mol was reported for GROMOS FF.[51] Finally, we compare H^{vap} from our simulation with experiments for alkylimidazolum and alkylpyrrolidinium cations paired with $N(CN)_2^-$ anions. Our predicted H^{vap} of 132 and 133.2 kJ/mol for [bmim][$N(CN)_2$] and [pyr_{12}][$N(CN)_2$], respectively, are lower than experimental values of 160 ± 2 kJ/mol for [pyr_{14}][$N(CN)_2$] and 157.2 ± 1.1 and 153.4 for [bmim][$N(CN)_2$] reported by Verevkin.[25]

5. Transport Properties

Self-Diffusion Coefficient. The self-diffusion coefficient D_i for species i was calculated using the Einstein relation:

$$D_i = \lim_{t\to\infty} \frac{\langle \mathrm{MSD}(t) \rangle}{6t} \tag{13}$$

where MSD(t) is mean-square displacement of a molecule (of type i) center-of-mass during time t and the broken brackets

denote an ensemble average. An example of the MSD(t) for [bmim][CF_3SO_3] at 393, 333, and 298 K is shown in the Supporting Information. Because of the finite size of the simulation cell, long-range hydrodynamic interactions restrict diffusion.[106] The leading order finite size correction (FSC) to self-diffusion coefficient (change to delta ΔD^{FSC}) was found to be inversely proportional to the simulation box and is given by[106]

$$\Delta D^{FSC} = \frac{2.837 k_B T}{6\pi\eta L} \quad (14)$$

where k_B is the Boltzmann constant, T is temperature, L is a linear dimension of the simulation periodic cell, and η is viscosity. We utilized viscosity from MD simulations for calculating ΔD^{FSC} where available. For ILs, where viscosity was not calculated from MD simulations, an experimental viscosity was utilized for estimating the finite size correction due to k-vector restriction of hydrodynamic interactions. The finite size correction is typically around 10−20% for the most of the simulated electrolytes.

Figure 5 shows the temperature dependence of the cation and anion self-diffusion coefficients corrected for the finite simulation size using eq 14 (ΔD^{FSC}) for 10 ILs. An excellent agreement is observed between the self-diffusion coefficients from MD simulations and pfg-NMR experiments for [bmim][Ntf_2], [C_6mim][Ntf_2], [bmmim][Ntf_2], [emim][BF_4], [bmim][BF_4], and [pyr_{14}][Ntf_2]. A deviation between pfg-NMR and MD simulations data for [pyr_{13}][Ntf_2] at high temperature is most likely due to poor experimental data as such a dramatic increase of the ion self-diffusion coefficient was not observed for a very similar IL [pyr_{14}][Ntf_2] from pfg-NMR experiments and our simulations (also shown in Figure 5d). MD simulations predict a slightly lower ion self-diffusion coefficients for the [$piperd_{14}$][Ntf_2] over the temperature range of experiments and for [bmim][PF_6] at the lowest simulated temperature (298 K). A slightly higher self-diffusion coefficient is predicted for [emim][Ntf_2] compared to pfg-NMR data. Figure 5 also demonstrates that the activation energy is predicted well in MD simulations for all IL with an exception of [bmim][PF_6] at the lowest temperature.

Table 6 summarizes self-diffusion coefficients for all simulated ILs. No finite simulation cell correction has been applied to data in Table 5, instead the magnitude of the correction is given. The largest deviation of simulation and experimental data are on the order of 40−60% and observed for [bmim][CF_3SO_3], [$piper_{14}$][Ntf_2], [$pyrid_4$][BF_4], [bmim][PF_6] ILs. However, after a finite cell correction, which is typically 10−20%, is applied the deviation between the experimental and simulation data decreases to 20−40% for these ILs. This quality of an agreement between simulation and experiment is quite rarely observed in MD simulations of ILs with an exception of few works.[51,56,57] Note, while some other groups have reported a similar quality excellent agreement with experiments, the systems were not sufficiently equilibrated and transport data was extracted from the subdiffusive regime. For example, Wu et al.[46] has reported an excellent agreement for D_+ and D_- for [bmim][BF_4] with pfg-NMR experiments from 0.2 ns simulations at 298 K. Using the mean-squared displacements from our simulations we estimate that extracting the ion self-diffusion coefficient from the subdiffusive regime [100:150] ps will result in an overestimation of the magnitude of the self-diffusion coefficient by 50% compared to the correctly extracted value from the diffusive

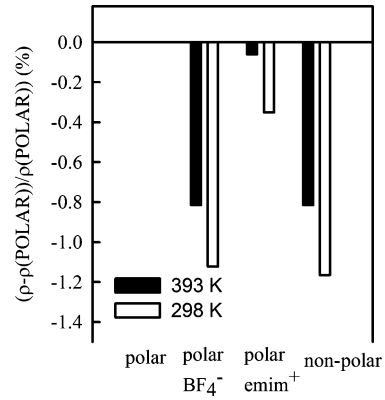

Figure 6. A relative density of [emim][BF_4] IL at 393 K from the following simulations: both ions are polarizable (polar), only BF_4^- or $emim^+$ were polarizable, polarization turned off (all nonpolar).

regime. Additional details on this topic are given in the Supporting Information of ref 62.

Ionic Conductivity. Ionic conductivity from MD simulations is calculated using the Einstein relation:

$$\lambda = \lim_{t\to\infty} \lambda^{app}(t) = \lim_{t\to\infty} \frac{e^2}{6tVk_BT} \sum_{i,j}^{n} z_i z_j \langle([\mathbf{R}_i(t) - \mathbf{R}_i(0)]) \times ([\mathbf{R}_j(t) - \mathbf{R}_j(0)])\rangle \quad (15)$$

where e is the electron charge, V is the volume of the simulation box, k_B is Boltzmann's constant, T is the temperature, t is time, z_i and z_j are the charges over ions i and j in electrons, $\mathbf{R}_i(t)$ is the displacement of the ion i during time t, the summation is performed over all ions, the broken brackets denote the ensemble average and N is the number of cations plus anions in the simulation cell. Here $\lambda^{app}(t)$ is the apparent time-dependent conductivity whose long-time limit corresponds to the equilibrium DC conductivity. Determining the long-time limit of $\lambda^{app}(t)$ using eq 15 is problematic even at high temperatures where the diffusion coefficients can be accurately determined because $\lambda^{app}(t)$, being a collective property, has poorer statistics and a higher uncertainty compared to MSD(t).

Conductivity can be decomposed into an "ideal" conductivity that would be realized if ion motion were uncorrelated, denoted $\lambda_{uncorr}(t)$, and the degree to which ion motion is in fact uncorrelated, or α_d. The degree of uncorrelated ion motion is given as the ratio of the collective (total) charge transport (λ)

$$\lambda^{app}_{uncorr} = \lim_{t\to\infty} \lambda^{app}_{uncorr}(t) = \lim_{t\to\infty} \frac{e^2}{6tVk_BT} \times \sum_{i}^{n} z_i^2 \langle[\mathbf{R}_i(t) - \mathbf{R}_i(0)]^2\rangle =$$

to the charge transport due to self-diffusion only (λ_{uncorr}):

$$= \frac{e^2}{Vk_BT}(n_+ D_+^{app} + n_- D_-^{app}) \quad (16)$$

$$\alpha_d = \frac{\lambda}{\lambda_{uncorr}} = \lim_{t\to\infty} \alpha_d(t) = \lim_{t\to\infty} \frac{\lambda^{app}(t)}{\lambda^{app}_{uncorr}(t)} \quad (17)$$

Here n_i is the number of atoms of type i = (cation or anion), $n = n_+ + n^-$. The degree of ion uncorrelated motion $\alpha_d = 1$ corresponds to completely uncorrelated ion motion, while α_d

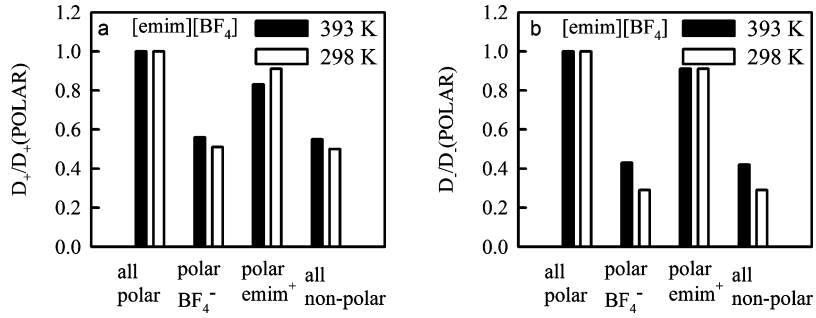

Figure 7. Cation (a) and anion (b) self-diffusion coefficients for [emim][BF_4] from the following simulations: both ions are polarizable (polar), only BF_4^- or $emim^+$ were polarizable, polarization turned off (all nonpolar).

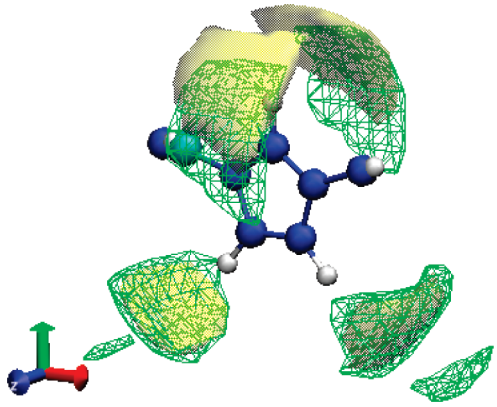

Figure 8. Isosurface of F atom of BF_4^- anion for $\rho/\rho^{random} = 4.5$ (volume distribution function) for [emim][BF_4] at 393 K. Solid isosurface corresponds to the polarizable model, wireframe isosurface—only BF_4^- is polarizable ($emim^+$ polarization turned off).

$= 0$ occurs if all of the cations only move together with anions. For practical reasons we first determine α_d from the apparent $\alpha_d(t)$ and use it to determine the conductivity. Our experience indicates that $\alpha_d(t)$ results are accurate only up to times approximately 2−5% of the total simulation run, consistent with similar claims for extracting viscosity from MD simulations.[107] We found that the degree of uncorrelated motion α_d lies in the narrow range of 0.58−0.85 for the investigated ILs. Similar values of α_d (0.52−0.78) have been reported[17,19,108] from the coordinated pfg-NMR and conductivity measurements of [emim][Ntf_2], [bmim][PF_6], [bmim][BF_4], [bmim][Ntf_2], [bmim][CF_3SO_3], [C_6mim][Ntf_2], [pyr_{14}][Ntf_2], [N_{1114}][Ntf_2], [pyrid$_4$][Ntf_2], and simulations.[59] The diffusion coefficients corrected for the finite simulation cell size were used for calculating conductivity of ILs that are given in Table 7 along with available experimental data.

The average absolute difference between the conductivity from MD simulations and experiments is 23%. For the majority of ILs the comparison of conductivity from MD simulations and experiments is consistent with the analysis of the self-diffusion coefficient presented above. The few exceptions are [bmmim][Ntf_2] and [pyr_{13}][Ntf_2] at 333 K. Bazito et al.[109] have reported an unusually low value for α_d of 0.4 for [bmmim][Ntf_2] from pfg-NMR and conductivity measurements, while MD simulations predict α_d of 0.55−0.6. Nicoreta et al.[110] also reported a quite low value α_d of 0.28 for [pyr_{13}][Ntf_2] at 333 K, while MD simulations predict α_d of 0.75 at 333 K. It is likely that these unusually low α_d are the reason for large deviations between the predicted from simulations conductivity and experimental values for these two ILs.

Viscosity. The equilibrium (zero shear rate) viscosity was calculated for a selected set of ILs with the longest NVT production runs using the Einstein relation including both diagonal and nondiagonal elements to enhance statistics,[111−113]

$$\eta = \lim_{t\to\infty} \eta(t) = \lim_{t\to\infty} \frac{V}{20k_BTt}\left\langle \sum_{\alpha,\beta} (L_{\alpha\beta}(t) - L_{\alpha\beta}(0))^2 \right\rangle \quad (18)$$

where $L_{\alpha\beta}(t) = \int_0^t P_{\alpha\beta}(t')\,dt'$, k_B is the Boltzmann constant, T is temperature, t is time, V is the volume of the simulation box, and P_{ab} is the stress sensor given by

$$P_{\alpha\beta} = \frac{\sigma_{\alpha\beta} + \sigma_{\beta\alpha}}{2} - \frac{\delta_{\alpha\beta}}{3} tr(\sigma) \quad (19)$$

where $\sigma_{\alpha\beta}$ is the stress tensor, $\delta_{\alpha\beta} = 1$ for $\alpha = \beta$, $\delta_{\alpha\beta} = 0$ for $\alpha \neq \beta$. Note that in our previous work[114] eq 19 was used for calculating viscosity and ω was set to 1 in eq 2 in ref 114. The apparent viscosity vs time is shown in the Supporting Information.

Viscosity extracted from MD simulations agree very well with experiments with deviations of less than 33% for most ILs as shown in Table 8. The exceptions are [bmim][NO_3] (for f1c version), [pyr_{12}][$N(CN)_2$] and [emim][$B(CN)_4$], [pyr_{13}][FSI(no Lp)] ILs for which MD simulation predictions of viscosity are 40−100% higher than experimental data. A revised f1e12 force field version for [bmim][NO_3] yields 2.2−2.4 times faster self-diffusion coefficients at 333 K as shown in Table 6, thus it is likely that a good agreement will be observed for viscosity of [bmim][NO_3] at 333 K for this FF version.

It is interesting to note that an excellent prediction of the ion self-diffusion coefficients, conductivity, and viscosity often correlates well with the quality of predicting H^{vap} from MD simulations. For example, an excellent agreement between MD simulations and experiments for the ion self-diffusion coefficients for [bmim][Ntf_2], [C_6mim][Ntf_2], and [bmim][BF_4] is consistent with an excellent agreement of simulation data and experiments observed for H^{vap}. Also slightly higher ion diffusion coefficients and conductivity for [emim][Ntf_2] are consistent with a slightly lower H^{vap} predicted from MD simulations compared to experiments. This analogy between the quality of predicting H^{vap} and transport properties does not hold, however, for [bmim][PF_6] and [bmim][$N(CN)_2$] at 298 K.

Influence of the Simulation Cell Size on Transport Properties. The influence of the finite simulation cell size on the IL transport properties has been investigated for [pyr_{13}][FSI(noLp)] at 393 K. Two simulation cells have been used containing 100 and 216 ion pairs. We have found that the ion self-diffusion coefficients of [pyr_{13}][FSI(noLp)] from simulations with a smaller box were 5% lower than the self-diffusion

coefficients extracted from simulations of a larger box. The slower ion self-diffusion for the smaller box is attributed to hydrodynamic interactions and could be recovered using eq 14. Viscosity [pyr_{13}][FSI(noLp)] was different for two simulation box sizes by only 8%. This difference is comparable to the error bar for extracting the viscosity from MD simulations. Thus, we do not observe any nonhydrodynamic effects due to a finite simulation box on ion self-diffusion coefficient or viscosity for the investigated range of box sizes from 34 to 44 Å. We cannot comment on the influence of the simulation box size for much larger box sizes as reported by the Margulis group.[115]

6. The Influence of Polarization of Ionic Liquid Structure and Transport

Understanding the influence of the many-body polarizable interactions on IL properties is important not only for achieving accurate property prediction from MD simulations but also for tailoring IL properties by selecting chemical groups with different polarizabilities. To improve understanding of the influence that atom and molecular polarizabilities have on the structural and transport properties of ILs, four MD simulations of [emim][BF_4] have been performed with polarizabilities of ions turned off and on as follows:

(a) Both cation and anion were polarizable (denoted "polar" in Figures 6 and 7).
(b) Only cation was polarizable (denoted "polar BF_4^-" in Figures 6 and 7).
(c) Only anion was polarizable (denoted "polar $emim^+$" in Figures 6 and 7).
(d) Both cations and anion were nonpolarizable (denoted "nonpolar" in Figures 6 and 7).

Figure 6 indicates that turning off cation polarization reduces IL density by 0.8%, thus creating more free volume in [emim][BF_4] in accord with previous results[44] for [emim][NO_3]. Turning off anion polarization, however, does not change IL density. Influence of the cation and anion polarization on the ion self-diffusion coefficients is shown in Figure 7. It is observed that turning off $emim^+$ polarization and leaving only BF_4^- polarizable results in a significant decrease of the ion self-diffusion coefficient despite that IL specific volume increases. Turning off BF_4^- polarization and leaving only $emim^+$ polarizable, on the other hand, only slightly reduces ion dynamics indicating that polarization of the $emim^+$ cation is more important that polarization of the BF_4^- anion for facilitating ion transport. The influence of polarization on the ion transport increases with decreasing temperature indicating that a nonpolarizable force field will have a higher activation energy for transport properties vs $1/T$. The larger influence of the $emim^+$ polarization on the ion dynamics compared to BF_4^- is consistent with a larger polarizability of $emim^+$ 11.1 $Å^3$ compared to 3.0 $Å^3$ molecular polarizability of BF_4^- as used in the developed force field. A similar extent of slowing down on ion transport upon turning off ion polarizability of ILs has been previously reported[44] for [emim][NO_3].

To provide a clue to the observed decrease of ion dynamics with increasing free volume we turn our attention to analyzing the structure, namely, to the analysis of a three-dimensional distribution of fluorine atoms of BF_4^- around $emim^+$ as shown in Figure 8. Examination of this figure indicates that the preferred position of BF_4^- anion near C_2 atom of $emim^+$ is noticeably different for the nonpolarizable and polarizable force fields. Specifically, turning off polarization results in the most probable anion positions from both sides of $emim^+$ being further apart compared to their locations from MD simulations using a polarizable force field. We also find that the BF_4^- local density above the C_2 carbon of $emim^+$ is lower for the nonpolarizable force field than for the polarizable force field. This lower local density indicates a higher free energy for BF_4^- to be located above C_2, therefore for the nonpolarizable model there is a higher free energy barrier that BF_4^- has to overcome during its jump from one side of $emim^+$ to another. In summary, turning off ion polarization increases free volume in IL but results in the structural changes consistent with the slowing down of ion dynamics.

7. Conclusions

A quantum chemistry-based polarizable force field has been developed and validated for a wide set of commonly used ILs and organic molecules. We observed an accurate description/prediction of density, heat of vaporization, self-diffusion coefficients, ionic conductivity, and viscosity of small organic molecules and ILs. A limited testing of the ability of the developed force field to predict ionic crystal lattice parameters indicated the force field applicability not only to liquid state properties but also to crystals. A set repulsion−dispersion parameters utilized during force field construction has exhibited good transferability. Two force fields were developed for FSI^- anion: (a) with an extended charge to achieve better description of electrostatic potential around FSI^- and (b) without extended charge. Simulations of [emim][FSI] and [pyr_{13}][FSI] using two representations of FSI^- anion yielded essentially the same densities and similar (within 20%) self-diffusion coefficients.

An investigation of the influence of the finite simulation box size on the ion self-diffusion and viscosity was studied for box sizes ranging from 34 to 44 Å. We found that a slight slowing down of ion dynamics observed for a smaller box size could be attributed to the hydrodynamic effects and is only 5%. The influence of polarization on [emim][BF_4] structure and ion transport has been investigated. Polarization of a larger $emim^+$ was found more important than polarization of a smaller BF_4^- anion for correct prediction of IL structure and transport. Turning off polarization resulted in a slight increase of IL volume accompanied by a decrease of ion transport, which was partially attributed to the changes of IL structure.

Acknowledgment. The authors are grateful for financial support of this work by Air Force Office of Scientific Research, Department of the Air Force contract number FA9550-09-C-0110 to Wasatch Molecular Inc. U.S. Department of Energy under Contract No. DE-AC02-05CH11231 on PO No. 6838611 to University of Utah is also acknowledged for support of ILs with FSI^- anion. Opinions, interpretations, conclusions, and recommendations are those of the authors and are not necessarily endorsed by the United States Air Force and DOE. An allocation of computer time from the Center for High Performance Computing at the University of Utah is gratefully acknowledged. Helpful discussions and suggestions from Wesley Henderson (NCSU), John Kerr (LBNL), Grant Smith (U. Utah), Jerry Boatz (AFRL), Ed Maginn (U. Notre Dame), Michel Armand, Todd Yeates (ARFL), Dmitry Bedrov (U. Utah), Stefan Schneider (AFRL) are highly appreciated.

Supporting Information Available: Length of production runs, definition of atom types, apparent viscosities, mean-square displacement, the degree of dynamic ion correlation for a selected set of ILs. This material is available free of charge via the Internet at http://pubs.acs.org.

References and Notes

(1) Smiglak, M.; Metlen, A.; Rogers, R. D. *Acc. Chem. Res.* **2007**, *40*, 1182–1192.

(2) Forsyth, S. A.; Pringle, J. M.; MacFarlane, D. R. *Aust. J. Chem.* **2004**, *57*, 113–119.

(3) Jin, C. M.; Ye, C. F.; Phillips, B. S.; Zabinski, J. S.; Liu, X. Q.; Liu, W. M.; Shreeve, J. M. *J. Mater. Chem.* **2006**, *16*, 1529–1535.

(4) Zeng, Z.; Phillips, B. S.; Xiao, J. C.; Shreeve, J. M. *Chem. Mater.* **2008**, *20*, 2719–2726.

(5) Shin, J. H.; Henderson, W. A.; Passerini, S. *Electrochem. Commun.* **2003**, *5*, 1016–1020.

(6) Garcia, B.; Lavallee, S.; Perron, G.; Michot, C.; Armand, M. *Electrochim. Acta* **2004**, *49*, 4583–4588.

(7) Galinski, M.; Lewandowski, A.; Stepniak, I. *Electrochim. Acta* **2006**, *51*, 5567–5580.

(8) De Long, H. C.; Trulove, P. C.; Sutto, T. E. *Ionic Liquids as Green Solvents: Progress and Prospects*; ACS Symposium Series 856; American Chemical Society: Washington, DC, 2003; pp 478−494.

(9) Ding, J.; Zhou, D.; Spinks, G.; Wallace, G.; Forsyth, S.; Forsyth, M.; MacFarlane, D. Use of Ionic Liquids as Electrolytes in Electromechanical Actuator Systems Based on Inherently Conducting Polymers. *Chem. Mater.* **2003**, *15*, 2392–2398.

(10) Cho, M. S.; Seo, H. J.; Nam, J. D.; Choi, H. R.; Koo, J. C.; Song, K. G.; Lee, Y. *Sens. Actuators, B* **2006**, *119*, 621–624.

(11) Liu, Y.; Shi, L. H.; Wang, M. J.; Li, Z. Y.; Liu, H. T.; Li, J. H. *Green Chem.* **2005**, *7*, 655–658.

(12) Hough, W. L.; Rogers, R. D. *Bull. Chem. Soc. Jpn.* **2007**, *80*, 2262–2269.

(13) Marsh, K. N.; Deev, A.; Wu, A. C. T.; Tran, E.; Klamt, A. *Korean J. Chem. Eng.* **2002**, *19*, 357–362.

(14) Schneider, S.; Hawkins, T.; Rosander, M.; Vaghjiani, G.; Chambreau, S.; Drake, G. *Energy Fuels* **2008**, *22*, 2871–2872.

(15) Fox, D. M.; Awad, W. H.; Gilman, J. W.; Maupin, P. H.; De Long, H. C.; Trulove, P. C. *Green Chem.* **2003**, *5*, 724–727.

(16) Tokuda, H.; Tabata, S. I.; Susan, M. A. B. H.; Hayamizu, K.; Watanabe, M. *J. Phys. Chem. B* **2004**, *108*, 11995–12002.

(17) Tokuda, H.; Hayamizu, K.; Ishii, K.; Abu Bin Hasan Susan, M.; Watanabe, M. *J. Phys. Chem. B* **2004**, *108*, 16593–16600.

(18) Singh, R. P.; Verma, R. D.; Meshri, D. T.; Shreeve, J. M. *Angew. Chem., Int. Ed.* **2006**, *45*, 3584–3601.

(19) Tokuda, H.; Hayamizu, K.; Ishii, K.; Susan, M. A. B. H.; Watanabe, M. *J. Phys. Chem. B* **2005**, *109*, 6103–6110.

(20) Tokuda, H.; Tsuzuki, S.; Susan, M. A. B. H.; Hayamizu, K.; Watanabe, M. *J. Phys. Chem. B* **2006**, *110*, 19593–19600.

(21) Kobrak, M. N. *Green Chem.* **2008**, *10*, 80–86.

(22) Trohalaki, S.; Pachter, R.; Drake, G. W.; Hawkins, T. *Energy Fuels* **2005**, *19*, 279–284.

(23) Krossing, I.; Slattery, J. M.; Daguenet, C.; Dyson, P. J.; Oleinikova, A.; Weingartner, H. *J. Am. Chem. Soc.* **2006**, *128*, 13427–13434.

(24) Gardas, R. L.; Coutinho, J. A. P. *Fluid Phase Equilib.* **2008**, *267*, 188–192.

(25) Verevkin, S. P. *Angew. Chem., Int. Ed.* **2008**, *47*, 5071–5074.

(26) Gardas, R. L.; Coutinho, J. A. P. *Fluid Phase Equilib.* **2008**, *263*, 26–32.

(27) Ye, C. F.; Shreeve, J. M. *J. Phys. Chem. A* **2007**, *111*, 1456–1461.

(28) Gardas, R. L.; Coutinho, J. A. P. *Fluid Phase Equilib.* **2008**, *266*, 195–201.

(29) Ye, C.; Shreeve, J. M. *J. Chem. Eng. Data* **2008**, *53*, 520–524.

(30) Hu, Z. H.; Margulis, C. J. *Proc. Natl. Acad. Sci. U.S.A.* **2006**, *103*, 831–836.

(31) Bhargava, B. L.; Balasubramanian, S. *J. Chem. Phys.* **2005**, *123*, 144505.

(32) Shah, J. K.; Maginn, E. J. *J. Phys. Chem. B* **2005**, *109*, 10395–10405.

(33) Del Popolo, M. G.; Lynden-Bell, R. M.; Kohanoff, J. *J. Phys. Chem. B* **2005**, *109*, 5895–5902.

(34) Lynden-Bell, R. M.; Kohanoff, J.; Del Popolo, M. G. *Faraday Discuss.* **2005**, *129*, 57–67.

(35) Kunsagi-Mate, S.; Lemli, B.; Nagy, G.; Kollar, L. *J. Phys. Chem. B* **2004**, *108*, 9246–9250.

(36) Antony, J. H.; Mertens, D.; Breitenstein, T.; Dolle, A.; Wasserscheid, P.; Carper, W. R. *Pure Appl. Chem.* **2004**, *76*, 255–261.

(37) Del Popolo, M. G.; Voth, G. A. *J. Phys. Chem. B* **2004**, *108*, 1744–1752.

(38) de Andrade, J.; Boes, E. S.; Stassen, H. *J. Phys. Chem. B* **2002**, *106*, 13344–13351.

(39) Jensen, M. P.; Neuefeind, J.; Beitz, J. V.; Skanthakumar, S.; Soderholm, L. *J. Am. Chem. Soc.* **2003**, *125*, 15466–15473.

(40) Lopes, C. J. N.; Deschamps, J.; Padua, A. A. H. *J. Phys. Chem. B* **2004**, *108*, 2038–2047.

(41) Lopes, J. N. C.; Deschamps, J.; Padua, A. A. H. *Ionic Liquids IIIA: Fundamentals, Progress, Challenges, and Opportunities, Properties and Structure*; ACS Symposium Series 901; 2005; pp 134−149.

(42) Morrow, T. I.; Maginn, E. J. *J. Phys. Chem. B* **2002**, *106*, 12807–12813.

(43) Shah, J. K.; Brennecke, J. F.; Maginn, E. J. *Green Chem.* **2002**, *4*, 112–118.

(44) Yan, T. Y.; Burnham, C. J.; Del Popolo, M. G.; Voth, G. A. *J. Phys. Chem. B* **2004**, *108*, 11877–11881.

(45) Deschamps, J.; Padua, A. A. H. *Ionic Liquids IIIA: Fundamentals, Progress, Challenges, and Opportunities, Properties and Structure*; ACS Symposium Series 901; 2005; pp 150−158.

(46) Wu, X. P.; Liu, Z. P.; Huang, S. P.; Wang, W. C. *Phys. Chem. Chem. Phys.* **2005**, *7*, 2771–2779.

(47) de Andrade, J.; Boes, E. S.; Stassen, H. *Ionic Liquids IIIA: Fundamentals, Progress, Challenges, and Opportunities, Properties and Structure*; ACS Symposium Series 901; 2005; pp 118−133.

(48) CanongiaLopes, J. N. A.; Padua, A. A. H. *J. Phys. Chem. B* **2006**, *110*, 7485–7489.

(49) Hunt, P. A. *Mol. Simul.* **2006**, *32*, 1–10.

(50) Deetlefs, M.; Hardacre, C.; Nieuwenhuyzen, M.; Padua, A. A. H.; Sheppard, O.; Soper, A. K. *J. Phys. Chem. B* **2006**, *110*, 12055–12061.

(51) Micaelo, N. M.; Baptista, A. M.; Soares, C. M. *J. Phys. Chem. B* **2006**, *110*, 14444–14451.

(52) CanongiaLopes, J. N.; CostaGomes, M. F.; Padua, A. A. H. *J. Phys. Chem. B* **2006**, *110*, 16816–16818.

(53) Rey-Castro, C.; Vega, L. F. *J. Phys. Chem. B* **2006**, *110*, 14426–14435.

(54) Cadena, C.; Anthony, J. L.; Shah, J. K.; Morrow, T. I.; Brennecke, J. F.; Maginn, E. J. *J. Am. Chem. Soc.* **2004**, *126*, 5300–5308.

(55) Siqueira, L. J. A.; Ribeiro, M. C. C. *J. Phys. Chem. B* **2007**, *111*, 11776−11785.

(56) Bhargava, B. L.; Balasubramanian, S. *J. Chem. Phys.* **2007**, *127*, 114510.

(57) Koddermann, T.; Paschek, D.; Ludwig, R. *Chemphyschem* **2007**, *8*, 2464–2470.

(58) Bhargava, B. L.; Balasubramanian, S.; Klein, M. L. *Chem. Commun.* **2008**, 3339–3351.

(59) Picálek, J.; Kolafa, J. *J. Mol. Liq.* **2007**, *134*, 29–33.

(60) Cadena, C.; Zhao, Q.; Snurr, R. Q.; Maginn, E. J. *J. Phys. Chem. B* **2006**, *110*, 2821–2832.

(61) CanongiaLopes, J. N.; Padua, A. A. H. *J. Phys. Chem. B* **2004**, *108*, 16893–16898.

(62) Borodin, O.; Smith, G. D. *J. Phys. Chem. B* **2006**, *110*, 11481–11490.

(63) Borodin, O.; Smith, G. D.; Henderson, W. *J. Phys. Chem. B* **2006**, *110*, 16879–16886.

(64) Cadena, C.; Maginn, E. J. *J. Phys. Chem. B* **2006**, *110*, 18026–18039.

(65) Jiang, W.; Yan, T. Y.; Wang, Y. T.; Voth, G. A. *J. Phys. Chem. B* **2008**, *112*, 3121–3131.

(66) Zhou, G. H.; Liu, X. M.; Zhang, S. J.; Yu, G. G.; He, H. Y. *J. Phys. Chem. B* **2007**, *111*, 7078–7084.

(67) Adebahr, J.; Grozema, F. C.; deLeeuw, S. W.; MacFarlane, D. R.; Forsyth, M. *Solid State Ionics* **2006**, *177*, 2845–2850.

(68) Schurhammer, R.; Wipff, G. *J. Phys. Chem. B* **2007**, *111*, 4659–4668.

(69) Siqueira, L. J. A.; Ribeiro, M. C. C. *J. Phys. Chem. B* **2007**, *111*, 11776–11785.

(70) Urukova, I.; Vorholz, J.; Maurer, G. *J. Phys. Chem. B* **2005**, *109*, 12154–12159.

(71) Huang, X. H.; Margulis, C. J.; Li, Y. H.; Berne, B. J. *J. Am. Chem. Soc.* **2005**, *127*, 17842–17851.

(72) Wang, Y. T.; Voth, G. A. *J. Phys. Chem. B* **2006**, *110*, 18601–18608.

(73) Wang, Y. T.; Voth, G. A. *J. Am. Chem. Soc.* **2005**, *127*, 12192–12193.

(74) Bresme, F.; Alejandre, J. *J. Chem. Phys.* **2003**, *118*, 4134–4139.

(75) Wu, X. P.; Liu, Z. P.; Wang, W. C. *Acta Phys.-Chim. Sin.* **2005**, *21*, 1138–1142.

(76) Liu, Z. P.; Wu, X. P.; Wang, W. C. *Phys. Chem. Chem. Phys.* **2006**, *8*, 1096–1104.

(77) CanongiaLopes, J. N.; Padua, A. A. H. *J. Phys. Chem. B* **2006**, *110*, 19586–19592.

(78) Li, H.; Boatz, J. A.; Gordon, M. S. *J. Am. Chem. Soc.* **2008**, *130*, 392-+.

(79) Lopes, J. N. C.; Padua, A. A. H.; Shimizu, K. *J. Phys. Chem. B* **2008**, *112*, 5039–5046.

(80) Padua, J. N. C.; Shimnizu, K.; Padua, A. A. H.; Umebayashi, Y.; Fukuda, S.; Fujii, K.; Ishiguro, S. I. *J. Phys. Chem. B* **2008**, *112*, 1465–1472.

(81) CanongiaLopes, J. N. A.; Padua, A. A. H. *J. Phys. Chem. B* **2006**, *110*, 3330–3335.

(82) Bagno, A.; D'Amico, F.; Saielli, G. *J. Mol. Liq.* **2007**, *131*, 17–23.
(83) Canongia Lopes, J.; xe, N.; Shimizu, K.; Pa, x.; dua, A.; xed; lio, A. H.; Umebayashi, Y.; Fukuda, S.; Fujii, K.; Ishiguro, S.-i. *J. Phys. Chem. B* **2008**, *112*, 9449–9455.
(84) Santos, L. M. N. B. F.; Lopes, J. N. C.; Coutinho, J. A. P.; Esperanca, J. M. S. S.; Gomes, L. R.; Marrucho, I. M.; Rebelo, L. P. N. *J. Am. Chem. Soc.* **2007**, *129*, 284–285.
(85) Sambasivarao, S. V.; Acevedo, O. *J. Chem. Theory Comput.* **2009**, *5*, 1038–1050.
(86) Kelkar, M. S.; Maginn, E. J. *J. Phys. Chem. B* **2007**, *111*, 4867–4876.
(87) Kelkar, M. S.; Maginn, E. J. *J. Phys. Chem. B* **2007**, *111*, 9424–9427.
(88) Maginn, E. J. *Acc. Chem. Res.* **2007**, *40*, 1200–1207.
(89) Jayaraman, S.; Maginn, E. J. *J. Chem. Phys.* **2007**, *127*, 214504.
(90) Shi, W.; Maginn, E. J. *J. Phys. Chem. B* **2008**, *112*, 2045–2055.
(91) Cadena, C.; Anthony, J. L.; Shah, J. K.; Morrow, T. I.; Brennecke, J. F.; Maginn, E. J. *J. Am. Chem. Soc.* **2004**, *126*, 5300–5308.
(92) Borodin, O.; Smith, G. D. *J. Phys. Chem. B* **2006**, *110*, 6279–6292.
(93) Pierce, F.; Tsige, M.; Borodin, O.; Perahia, D.; Grest, G. S. *J. Chem. Phys.* **2008**, *128*, 214903–14.
(94) Borodin, O.; Smith, G. D. *J. Phys. Chem. B* **2006**, *110*, 6293–6299.
(95) Borodin, O.; Smith, G. D.; Fan, P. *J. Phys. Chem. B* **2006**, *110*, 22773–22779.
(96) Borodin, O.; Smith, G. D.; Geiculescu, O.; Creager, S. E.; Hallac, B.; DesMarteau, D. *J. Phys. Chem. B* **2006**, *110*, 24266–24274.
(97) Borodin, O.; Smith, G. D. *J. Phys. Chem. B* **2009**, *113*, 1763–1776.
(98) Miller, K. J.; Savchik, J. *J. Am. Chem. Soc.* **1979**, *101*, 7206–7213.
(99) Morita, A.; Kato, S. *J. Chem. Phys.* **1999**, *110*, 11987–11998.
(100) Ayyagari, C.; Bedrov, D.; Borodin, O.; Smith, G. D. Lucretius, MD simulation code http://www.eng.utah.edu/~gdsmith/lucretius.html. (accessed Jan 2009).
(101) Smith, G. D.; Borodin, O.; Li, L.; Kim, H.; Liu, Q.; Bara, J. E.; Gin, D. L.; Nobel, R. *Phys. Chem. Chem. Phys.* **2008**, *10*, 6301–6312.
(102) Armstrong, J. P.; Hurst, C.; Jones, R. G.; Licence, P.; Lovelock, K. R. J.; Satterley, C. J.; Villar-Garcia, I. J. *Phys. Chem. Chem. Phys.* **2007**, *9*, 982–990.
(103) Zaitsau, D. H.; Kabo, G. J.; Strechan, A. A.; Paulechka, Y. U.; Tschersich, A.; Verevkin, S. P.; Heintz, A. *J. Phys. Chem. A* **2006**, *110*, 7303–7306.
(104) Raabe, G.; Koehler, J. *J. Chem. Phys.* **2008**, *128*, 154509.
(105) Emel'yanenko, V. N.; Verevkin, S. P.; Heintz, A.; Schick, C. *J. Phys. Chem. B* **2008**, *112*, 8095–8098.
(106) Dunweg, B.; Kremer, K. *J. Chem. Phys.* **1993**, *99*, 6983–6997.
(107) Mondello, M.; Grest, G. S. *J. Chem. Phys.* **1997**, *106*, 9327–9336.
(108) Tokuda, H.; Ishii, K.; Susan, M. A. B. H.; Tsuzuki, S.; Hayamizu, K.; Watanabe, M. *J. Phys. Chem. B* **2006**, *110*, 2833–2839.
(109) Bazito, F. F. C.; Kawano, Y.; Torresi, R. M. *Electrochim. Acta* **2007**, *52*, 6427–6437.
(110) Nicotera, I.; Oliviero, C.; Henderson, W. A.; Appetecchi, G. B.; Passerini, S. *J. Phys. Chem. B* **2005**, *109*, 22814–22819.
(111) Daivis, P. J.; Evans, D. J. *J. Chem. Phys.* **1994**, *100*, 541–547.
(112) Mondello, M.; Grest, G. S. *J. Chem. Phys.* **1997**, *106*, 9327–9336.
(113) Bedrov, D.; Smith, G. D.; Sewell, T. D. *J. Chem. Phys.* **2000**, *112*, 7203–7208.
(114) Borodin, O.; Smith, G. D.; Kim, H. *J. Phys. Chem. B* **2009**, *113*, 4771–4774.
(115) Hu, Z.; Margulis, C. J. *Acc. Chem. Res.* **2007**, *40*, 1097–1105.
(116) http://webbook.nist.gov/chemistry/, NIST Webbook. In. (accessed March, 2009).
(117) Greiner-Schmid, A.; Wappmann, S.; Has, M.; Ludemann, H. D. *J. Chem. Phys.* **1991**, *94*, 5643–5649.
(118) Fishman, E. *J. Phys. Chem.* **1955**, *59*, 469–472.
(119) Mondello, M.; Grest, G. S. *J. Chem. Phys.* **1997**, *106*, 9327–9336.
(120) Parker, R. G.; Jonas, J. *J. Chem. Eng. Data* **1972**, *17*, 300–302.
(121) Garcia Baonza, V.; Caceres Alonso, M.; Nunez Delgado, J. *J. Phys. Chem.* **1992**, *96*, 1932–1938.
(122) The CRC Handbook of Chemistry and Physics, 2006−2007. http://www.hbcpnetbase.com/ (accessed 2006).
(123) Borodin, O.; Smith, G. D.; Bedrov, D. *J. Phys. Chem. B* **2002**, *106*, 9912–9922.
(124) Hayamizu, K.; Aihara, Y.; Arai, S.; Martinez, C. G. *J. Phys. Chem. B* **1999**, *103*, 519–524.
(125) Barthel, J.; Neueder, R.; Roch, H. *J. Chem. Eng. Data* **2000**, *45*, 1007–1011.
(126) Verevkin, S. P.; Emel'yanenko, V. N.; Toktonov, A. V.; Chernyak, Y.; Schaffner, B.; Borner, A. *J. Chem. Thermodyn.* **2008**, *40*, 1428–1432.
(127) Steele, W. V.; Chirico, R. D.; Knipmeyer, S. E.; Nguyen, A. *J. Chem. Eng. Data* **1997**, *42*, 1008–1020.
(128) Saha, N.; Das, B.; Hazra, D. K. *J. Chem. Eng. Data* **2000**, *45*, 353.
(129) Shiflett, M. B.; Yokozeki, A. *J. Chem. Eng. Data* **2007**, *52*, 1302–1306.
(130) Stoppa, A.; Hunger, J.; Buchner, R. *J. Chem. Eng. Data* **2009**, *54*, 472–479.
(131) Harris, K. R.; Kanakubo, M.; Woolf, L. A. *J. Chem. Eng. Data* **2007**, *52*, 1080–1085.
(132) Gardas, R. L.; Freire, M. G.; Carvalho, P. J.; Marrucho, I. M.; Fonseca, I. M. A.; Ferreira, A. G. M.; Coutinho, J. A. P. *J. Chem. Eng. Data* **2007**, *52*, 1881–1888.
(133) Seddon, K. R.; Stark, A.; Torres, M. J. *Clean Solvents* **2002**, *819*, 34–49.
(134) Blanchard, L. A.; Gu, Z. Y.; Brennecke, J. F. *J. Phys. Chem. B* **2001**, *105*, 2437–2444.
(135) Zhou, Z. B.; Matsumoto, H.; Tatsumi, K. *Chemphyschem* **2005**, *6*, 1324–1332.
(136) Yoshida, Y.; Baba, O.; Saito, G. *J. Phys. Chem. B* **2007**, *111*, 4742–4749.
(137) Fredlake, C. P.; Crosthwaite, J. M.; Hert, D. G.; Aki, S.; Brennecke, J. F. *J. Chem. Eng. Data* **2004**, *49*, 954–964.
(138) Zhang, S.; Sun, N.; He, X.; Lu, X.; Zhang, X. *J. Phys. Chem. Ref. Data* **2006**, *35*, 1475–1517.
(139) Yoshida, Y.; Muroi, K.; Otsuka, A.; Saito, G.; Takahashi, M.; Yoko, T. *Inorg. Chem.* **2004**, *43*, 1458–1462.
(140) MacFarlane, D. R.; Meakin, P.; Sun, J.; Amini, N.; Forsyth, M. *J. Phys. Chem. B* **1999**, *103*, 4164–4170.
(141) Zhou, Z. B.; Matsumoto, H.; Tatsumi, K. *Chem.—Eur. J.* **2006**, *12*, 2196–2212.
(142) Tsunashima, K.; Sugiya, M. *Electrochem. Commun.* **2007**, *9*, 2353–2358.
(143) Zhou, Z. B.; Matsumoto, H.; Tatsumi, K. *Chem.—Eur. J.* **2006**, *12*, 2196–2212.
(144) Gu, Z. Y.; Brennecke, J. F. *J. Chem. Eng. Data* **2002**, *47*, 339–345.
(145) Choudhury, A. R.; Winterton, N.; Steiner, A.; Cooper, A. I.; Johnson, K. A. *Crystengcomm* **2006**, *8*, 742–745.
(146) Henderson, W. A. (NCSU) manuscript in preparation.
(147) Choudhury, A. R.; Winterton, N.; Steiner, A.; Cooper, A. I.; Johnson, K. A. *J. Am. Chem. Soc.* **2005**, *127*, 16792–16793.
(148) Kanakubo, M.; Harris, K. R.; Tsuchihashi, N.; Ibuki, K.; Ueno, M. *J. Phys. Chem. B* **2007**, *111*, 2062–2069.
(149) Noda, A.; Hayamizu, K.; Watanabe, M. *J Phys Chem B* **2001**, *105*, 4603–4610.
(150) Zhou, Z. B.; Matsumoto, H.; Tatsumi, K. *Chem. Lett.* **2004**, *33*, 680–681.
(151) Matsumoto, H.; Sakaebe, H.; Tatsumi, K.; Kikuta, M.; Ishiko, E.; Kono, M. *J. Power Sources* **2006**, *160*, 1308–1313.
(152) Wang, Y. D.; Zaghib, K.; Guerfi, A.; Bazito, F. F. C.; Torresi, R. M.; Dahn, J. R. *Electrochim. Acta* **2007**, *52*, 6346–6352.
(153) Zhou, Q.; Henderson, W. A.; Appetecchi, G. B.; Montanino, M.; Passerini, S. *J. Phys. Chem. B* **2008**, *112*, 13577–13580.
(154) Bai, Y.; Cao, Y. M.; Zhang, J.; Wang, M.; Li, R. Z.; Wang, P.; Zakeeruddin, S. M.; Gratzel, M. *Nat. Mater.* **2008**, *7*, 626–630.
(155) Pitner, W. R.; Ignat'ev, N. Ionic Liquids for Electrochemical Applications. 214th Electrochemical Society Meeting, Honolulu, Hawaii, October, 12-17, 2008.
(156) Hayamizu, K.; Aihara, Y.; Nakagawa, H.; Nukuda, T.; Price, W. S. *J. Phys. Chem. B* **2004**, *108*, 19527–19532.

JP905220K